Modeling and Applications of Tridimensional Acoustic Standing Waves

Louis-Jacques Bourdages

Department of Mechanical Engineering

McGill University, Montreal

September 2023

A thesis submitted to McGill University in partial fulfillment of the requirement of the degree of Master of Engineering

Abstract

Ultrasonic acoustic resonance has found diverse applications in various scientific and industrial fields, leveraging its ability to manipulate sound waves and propagate energy. These sound waves have properties making them uniquely suited to a range of tasks which will be reviewed and studied in this work. Contactless force application, or acoustophoresis, is one such use of the acoustic pressure generated by the sound waves which is assessed. Another phenomenon discussed is cavitation generated with high amplitude acoustic waves, where accurate control of bubble inception presents opportunities for various applications in sonochemistry, including hydrogel polymerization. To precisely engineer the location and strength of those points of high pressure, a resonant acoustic chamber ~~can be used~~is developed. These areas can be shaped according to periodic patterns by exploiting the modes of vibration of the acoustic chamber. The design parameters of the acoustic chambers and the excitation frequency are tuned to create chambers with optimized resonance characteristics. This is accomplished through numerical optimization algorithms and FEM models of the chambers. Using the output of those optimizations, experimental setups replicating the simulations are created and the acoustic resonance is quantified with ultrasonic probes to validate the accuracy of said simulations. With precise models, good agreement is found between the simulated and empirical pressure fields. The limitations of those models are also investigated by studying the effect of cavitation bubbles on the acoustic chamber's resonance. Cavitation bubbles are theorized to dampen the transmission of traveling sound waves, inhibiting resonance within the chambers. To verify this point, a liquid-filled chamber is designed and simulated, and the cavitation field of a matching experimental chamber is observed through sonoluminescence. By comparing the experimental and simulated results, the damping effect of cavitation on resonance is observed.

Commented [JL2]: Revise to clearly show two applications. The current version is unclear.

Commented [JL3]: An ending sentence about the overall implication and future applications.

Potential applications of these techniques are explored with additional models. Acoustophoretic printing is considered by simulating subwavelength acoustic resonators able to eject microscopic droplets onto a substrate. Resonance is achieved in those simulated cavities. Then, to investigate the patterning of acoustic features in a tridimensional acoustic field, a chamber implementing four identical subwavelength resonators is optimized and simulated. Finally, sonochemistry applications using these techniques are tested by creating gels through Sono-RAFT polymerization. One of those gels is presented. These results suggest engineered tridimensional acoustic fields may be further researched to develop novel manufacturing techniques.

Formatted: English (Canada)

Abrégé

La résonance acoustique ultrasonique a trouvée diverses applications dans de nombreux domaines scientifiques et industriels, en exploitant sa capacité à manipuler les ondes sonores et à propager l'énergie. Ces ondes sonores ont des propriétés qui les rendent particulièrement adaptées à une série de tâches qui seront examinées et étudiées dans ce document. L'application d'une force sans contact, ou acoustophorèse, est l'une des utilisations de la pression acoustique générée par les ondes sonores qui est évaluée. Un autre phénomène abordé est la cavitation générée par des ondes acoustiques de grande amplitude, où le contrôle précis de l'apparition des bulles offre des possibilités pour diverses applications en sonochimie, y compris la polymérisation des hydrogels. Pour déterminer avec précision l'emplacement et la force de ces points de haute pression, on peut utiliser une chambre acoustique résonante. Ces zones peuvent être répétées périodiquement en exploitant les modes de vibration de la chambre acoustique. Les dimensions des chambres acoustiques et la fréquence d'excitation sont ajustées pour optimiser les caractéristiques de résonance. Pour ce faire, on utilise des algorithmes d'optimisation numérique et des modèles FEM. En utilisant les résultats de ces optimisations, des appareils expérimentaux reproduisant les simulations sont créés et la résonance acoustique est quantifiée à l'aide de sondes ultrasoniques afin de valider la précision de ces simulations. Avec des modèles précis, on constate une bonne concordance entre les champs de pression simulés et empiriques. Les limites de ces modèles sont également examinées en étudiant l'effet des bulles de cavitation sur la résonance de la chambre acoustique. Les bulles de cavitation sont censées atténuer la transmission des ondes sonores qui se déplacent, inhibant ainsi la résonance dans les chambres. Pour le vérifier, une chambre remplie de liquide est conçue et simulée, et le champ de cavitation d'une chambre expérimentale correspondante est observé par

sonoluminescence. En comparant les résultats expérimentaux et simulés, on observe l'effet inhibant de la cavitation sur la résonance. Les applications potentielles de ces techniques sont explorées à l'aide de modèles supplémentaires. L'impression acoustophorétique est considérée en simulant des résonateurs acoustiques plus petits que la longueur d'onde capables d'éjecter des gouttelettes microscopiques sur un substrat. La résonance est obtenue dans ces cavités simulées. Ensuite, pour étudier le modelage de caractéristiques acoustiques dans un champ acoustique tridimensionnel, une chambre mettant en œuvre quatre résonateurs identiques est optimisée et simulée. Enfin, les applications sonochimiques de ces techniques sont testées en créant des gels par polymérisation Sono-RAFT. L'un de ces gels est présenté. Ces résultats suggèrent que les champs acoustiques tridimensionnels peuvent faire l'objet de recherches plus approfondies afin de mettre au point de nouvelles techniques de fabrication.

Formatted: French (Haiti)

Acknowledgements

We thank Jianyu Li, Luc Mongeau, Zixin He, Zhen Yang, Ran Huo, Evan Johnston, Yixun Cheng, Kaustuv Basu, Shiyu Liu and Ran Huo for their experimental assistance, academic support and discussions.

We also thank Lyle G. Whyte, Catherine Maggiori, Isabelle Raymond-Bouchard, Miguel Angel Fernandez Martinez, Brady O’Conor, Scott Sugden, Olivia Blenner-Hassett for the academic opportunities afforded by my work with them.

Commented [JL4]: More to develop

Commented [JL5R4]: Please add

Commented [JL6R4]: For instance ,you can also mention your team in Mac campus. Thank the people you like to acknowledge.

Table of Contents

Formatted: English (Canada)

Abstract II

Abrégé IV

Acknowledgements VI

Table of Contents VII

List of Figures XII

List of Tables XX

List of Abbreviations XX

Contribution of Authors XXI

Chapter 1. Introduction 1

1.1. Background 1

1.2. Thesis Structure 4

Chapter 2. Literature Review 5

2.1. Acoustics 5

2.1.1. Introduction 5

2.2. Acoustophoretics 8

2.2.1. Introduction 8

2.2.2. Applications of Acoustophoretics 9

2.3. Cavitation 14

2.3.1. Introduction 14

2.3.2. Applications of Cavitation 16

2.4. Finite Element Modeling 18

2.4.1. Introduction 18

Chapter 3. Finite Element Modeling for the Analysis of Ultrasonic Acoustic Fields 22

3.1. Numerical Models Setup 22

3.2. Results and Discussion 28

3.2.1. Fabry-Perot Resonator Simulation...28

3.2.2. Resonator Array Simulation 32

3.2.3. Resonant Chamber 34

3.2.4. Water-filled Resonant Chamber 37

Chapter 4. Direct Measurement of Acoustic Fields and Cavitation Characterization through SCL 39

4.1. Experimental Section 39

4.1.1. Sound Pressure Measurement 39

4.1.2. Sonochemiluminescence 42

4.1.3 Gel Polymerization Chambers 43

4.2. Results and Discussion 45

4.2.1. Resonant Chamber Analysis and FEM Validation 45

4.2.2. SCL Imagery 49

4.3. Demonstration of Potential Applications 51

Chapter 5. Conclusion and Recommendations 56

5.1. Conclusion 56

5.2. Recommendations 57

5.3. Original Contributions to Knowledge 58

References 60

~~Abstract ..... II~~

~~Abrégé ..... III~~

~~Acknowledgements ..... IV~~

~~Table of Contents ..... V~~

~~List of Figures ..... VII~~

~~List of Abbreviations ..... IX~~

~~Contribution of Authors ..... X~~

~~Chapter 1. Introduction ..... 1~~

~~1.1. Background ..... 1~~

~~1.2. Thesis Structure ..... 3~~

~~Chapter 2. Literature Review ..... 4~~

~~2.1. Acoustics ..... 4~~

~~2.1.1. Introduction ..... 4~~

~~2.2. Acoustophoretics ..... 6~~

~~2.2.1. Introduction ..... 6~~

~~2.2.2. Applications of Acoustophoretics ..... 7~~

~~2.3. Cavitation ..... 10~~

~~2.3.1. Introduction ..... 10~~

Formatted: Default Paragraph Font

Formatted: Default Paragraph Font, English (Canada)

Formatted: Default Paragraph Font

Formatted: Default Paragraph Font, English (Canada)

Formatted: Default Paragraph Font

Formatted: Default Paragraph Font

Formatted: Default Paragraph Font

Formatted: Default Paragraph Font, Check spelling and grammar

Formatted: Default Paragraph Font

Formatted: Default Paragraph Font, English (Canada)

Formatted: Default Paragraph Font, Check spelling and grammar

Formatted: Default Paragraph Font, English (Canada)

Formatted: Default Paragraph Font, Check spelling and grammar

Formatted: Default Paragraph Font, English (Canada)

Formatted: Default Paragraph Font, English (Canada), Check spelling and grammar

Formatted: Default Paragraph Font, English (Canada), Check spelling and grammar

Formatted: Default Paragraph Font, English (Canada)

Formatted: Default Paragraph Font, English (Canada), Check spelling and grammar

~~2.3.2. Applications of Cavitation ....12~~

~~2.4. Finite Element Modeling ....13~~

~~2.4.1. Introduction ....13~~

~~Chapter 3. Finite Element Modeling for the Analysis of Ultrasonic Acoustic Fields ....16~~

~~3.1. Numerical Models Setup ....16~~

~~3.2. Results and Discussion ....19~~

~~3.2.1. Fabry-Perot Resonator Simulation...19~~

~~3.2.2. Resonator Array Simulation ....21~~

~~3.2.3. Resonant Chamber ....23~~

~~3.2.4. Water-filled Resonant Chamber ....24~~

~~Chapter 4. Direct Measurement of Acoustic Fields and Cavitation Characterization through SCL ....26~~

~~4.1. Experimental Section...26~~

~~4.1.1. Sound Pressure Measurement...26~~

~~4.1.2. Sonochemiluminescence...27~~

~~4.2. Results and Discussion ....28~~

~~4.2.1. Resonant Chamber Analysis and FEM Validation...28~~

~~4.2.2. SCL Imagery...29~~

~~4.3. Applications ....30~~

~~Chapter 5. Conclusion and Recommendations...32~~

~~5.1. Conclusion ....32~~

Formatted: Default Paragraph Font, English (Canada), Check spelling and grammar

Formatted: Default Paragraph Font

Formatted: Default Paragraph Font, English (Canada), Check spelling and grammar

Formatted: Default Paragraph Font, Check spelling and grammar

Formatted: Default Paragraph Font

Formatted: Default Paragraph Font, English (Canada)

Formatted: Default Paragraph Font, English (Canada), Check spelling and grammar

Formatted: Default Paragraph Font, English (Canada), Check spelling and grammar

Formatted: Default Paragraph Font, English (Canada), Check spelling and grammar

Formatted: Default Paragraph Font, English (Canada), Check spelling and grammar

Formatted: Default Paragraph Font, Check spelling and grammar

Formatted: Default Paragraph Font

Formatted: Default Paragraph Font, English (Canada), Check spelling and grammar

Formatted: Default Paragraph Font, English (Canada), Check spelling and grammar

Formatted: Default Paragraph Font, English (Canada)

Formatted: Default Paragraph Font, English (Canada), Check spelling and grammar

Formatted: Default Paragraph Font, English (Canada), Check spelling and grammar

Formatted: Default Paragraph Font, English (Canada)

Formatted: Default Paragraph Font, English (Canada), Check spelling and grammar

Formatted: Default Paragraph Font, English (Canada)

~~5.2. Recommendations......32~~

~~5.3. Original Contributions to Knowledge......33~~

~~References......35~~

~~Appendix......38~~

Formatted: Default Paragraph Font, English (Canada)

Formatted: Default Paragraph Font, English (Canada)

Formatted: Default Paragraph Font, Check spelling and grammar

Formatted: Default Paragraph Font, English (Canada), Check spelling and grammar

List of Figures

Commented [JL7]: Page break?

Formatted: Heading 2, Tab stops: Not at 16.49 cm

Formatted: Indent: Left: 0 cm, Hanging: 1 cm

Figure 1 : Experiment comparing numerically simulated and empirical acoustic fields. Mapping of hydrophone measurements in plexiglass water-filled tanks at three different heights (a, b, c) (left) and simulation of acoustic pressure distribution within tank (right). (Reproduced from (28), copyright 2016, Elsevier) 7

Figure 2 : Acoustic tweezer designs. Schematic of acoustic manipulation device based on Bulk Acoustic Waves (a) and Surface Acoustic Waves (b) (Reproduced from (36), copyright 2019, IOP Publishing)....10

Figure 3 : Principle and acoustophoretic properties of the subwavelength resonator. (A) Schematic view of the subwavelength acoustophoretic voxel ejector (left). The resonance (schematically shown in red) leads to high acoustic pressure amplification while keeping the field strongly confined (right). (B) Side view of the experimental setup (top) and close-up of the tapered nozzle ($\lambda \approx 14$ mm) (bottom). Calculated vertical force distribution inside the subWAVE (C) and its experimental validation (D). (E) Schematic illustration of acoustophoretic printing. (F) Log-log plot of vertical force generated within the subWAVE as a function of drop volume compared to a classical standing-wave levitator. (Reproduced from (5), copyright 2018, AAAS)....12

Figure 4 : Generalized profiles for the strength of effects correlated to the mechanical shear forces generated from the collapsing bubble, and the reactive radicals formed from vapor molecule sonolysis. (Reproduced from (45), copyright 2019, Wiley-VCH) 16

Figure 5 : Hydrogel polymerization reaction summary. Scheme for Sono-RAFT polymerization (a). Molecular weight evolution characteristics with regards to

monomer conversion during Sono-RAFT polymerization (b). Protocol to complete the monomer conversion with periods of ultrasonic excitation denoted with a symbol and periods of pause excitation in grey (c). (Reproduced from (45), copyright 2019, Wiley-VCH) 18

Figure 6 : Schematic for chamber designed to excite an array of four Fabry-Pérot resonators. Note the location of the cylindrical ultrasonic transducer exciting the chamber (a), the extents of the acoustic chamber (a rectangular box) (b), the four cylindrical resonators (c) and the four corresponding surfaces used for the calculation of the far field absorption of the sound waves emitted, which are modeled as hemispheres. The hemispheres are modeled to provide enough space for the soundwave exiting the aperture to develop fully, which improves the accuracy of the far field absorption (d) See Figure 9 for a 3D view of the system...26

Figure 7 : Cross sectional view of the acoustic pressure field within a chamber excited by an ultrasonic sound source, with the inside of the chamber above and the open air below, both connected by the Fabry-Perot resonator. Pressure in Pa...31

Figure 8 : Pressure distribution along centerline of the 6.2 mm long Fabry-Pérot resonator, moving from the top (inside of the chamber) to the bottom (outside of the chamber). 32

Figure 9 : Plots representing the pressure field within the acoustic chamber designed to excite four resonators. All axes in units of Pascals. Plots (a), (b), and (c) show the acoustic pressure in the chamber on the bottom of the chamber (at the entrance of the resonators), halfway up the height of the acoustic chamber, and

on the top surface of the acoustic chamber, respectively. Plot (d) shows the isosurface plot of the acoustic pressure within the chamber. 34

Figure 10 : Iso-surface plot of the total acoustic pressure within the air-filled chamber as solved by the finite element model. 35

Figure 11 : FEM simulation of water-filled chamber during excitation by transducer located in the upper right corner of the chamber. The RMS acoustic pressure in Pascals is plotted. 37

Figure 12 : FEM model of the water-filled chamber. Isosurface plot showing the sound pressure in Pascals. 38

Figure 13 : Probe microphone in chamber on the left, including 3D-printed adapter (b) attached to ultrasonic transducer (a) and fused silica tubing (c) glued to the adapter. On the right, the tip of the probe inserted through the side of the chamber (d). 41

Figure 14 : Real color imagery of the luminol solution-filled chamber recorded during sonication, 5 minutes exposure time. (a) is the bounds of the chamber, (b) is the location of the transducer horn. 43

Figure 15 : Chamber used in first gel polymerization experiment. 44

Figure 16 : Chamber used in second gel polymerization experiment. 45

Figure 17 : Resonant chamber acoustic field comparative analysis. (a) Results of the FEM simulation of the air-filled acoustic chamber. The heatmap shows a regular pattern of pressure antinodes. The line plot below shows the pressure variation alongside a single edge of the vessel, displaying clearly peaks and troughs in the measurement. (b) RMS pressure measured with the probe microphone. The line plot below shows the pressure variation alongside a

single edge of the vessel, displaying peaks and troughs in the measurement. (c) Mapping of the relative error between the empirical and experimental RMS pressure. Blue regions are where the simulated pressure was much lower than the experimental, red are where it was much higher, white are where it was within +/-50% of the value. Many topological features are captured in both, including the pressure antinodes and the two hexagon-shaped features at 36 and 70 mm alongside the X axis..47

Figure 18 : Validation of the numerical model of an ultrasonic sonoreactor with experimental results (Reproduced from (61), copyright 2020, Elsevier)........49

Figure 19 : Processed data output of SCL experiment. (b) shows the raw light information in monochrome. Data along the red line is plotted in (a) and data along the blue line is plotted in (c). (d) shows the area of the graph where the luminosity recorded is more than 20% higher than the base luminosity recorded in the dark parts of the image (attributed to sensor noise). This area represents 1.707 cm^2. The "Light detected" axes in (a) and (b) range from 0 to 1, above which the camera sensor was overexposed. 50

Figure 20 : Images of hydrogels polymerized using ultrasound. (a) Set of three hydrogels polymerized in a closed vessel by applying an ultrasonic excitation for 5 minutes to a solution through the PET film at three points separated from each other by three centimeters. (b) Gel polymerized in a vessel through direct application of an ultrasonic excitation for 5 minutes. 53

~~**Figure 1** : Experiment comparing numerically simulated and empirical acoustic fields. Mapping of hydrophone measurements in plexiglass water-filled tanks at three different heights (a, b, c) (left) and simulation of acoustic~~

Formatted: Font: Not Italic

Formatted: Indent: Left: 1 cm, Hanging: 1 cm, Don't adjust right indent when grid is defined

~~pressure distribution within tank (right). (Reproduced from (26), copyright 2016, Elsevier)~~.....7

~~**Figure 2** : Acoustic tweezer designs. Schematic of acoustic manipulation device based on Bulk Acoustic Waves (a) and Surface Acoustic Waves (b) (Reproduced from (34), copyright 2019, IOP Publishing)~~.....9

~~**Figure 3** : Principle and acoustophoretic properties of the subwavelength resonator. (A) Schematic view of the subwavelength acoustophoretic voxel ejector (left). The resonance (schematically shown in red) leads to high acoustic pressure amplification while keeping the field strongly confined (right). (B) Side view of the experimental setup (top) and close-up of the tapered nozzle (λ ≈ 14 mm) (bottom). Calculated vertical force distribution inside the subWAVE (C) and its experimental validation (D). (E) Schematic illustration of acoustophoretic printing. (F) Log-log plot of vertical force generated within the subWAVE as a function of drop volume compared to a classical standing-wave levitator. (Reproduced from (5), copyright 2018, AAAS).~~.....11

~~**Figure 4** : Generalized profiles for the strength of effects correlated to the mechanical shear forces generated from the collapsing bubble, and the reactive radicals formed from vapor molecule sonolysis. (Reproduced from (43), copyright 2019, Wiley-VCH)~~.....13

~~**Figure 5** : Hydrogel polymerization reaction summary. Scheme for Sono-RAFT polymerization (a). Molecular weight evolution characteristics with monomer conversion during Sono-RAFT polymerization (b). Protocol to complete the monomer conversion with periods of ultrasonic~~

~~excitation denoted with a symbol and periods of pause excitation in grey (c). (Reproduced from (43), copyright 2019, Wiley-VCH)~~ 14

~~**Figure 6** : Schematic for chamber designed to excite an array of four Fabry-Pérot resonators. Note the location of the ultrasonic transducer exciting the chamber (a), the extents of the acoustic chamber (b), the four resonators (c) and the four corresponding surfaces used for the calculation of the far field absorption of the sound waves emitted (d).~~.....................20

~~**Figure 7** : Cross sectional view of the acoustic pressure field within a chamber excited by an ultrasonic sound source, with the inside of the chamber above and the open air below, both connected by the Fabry-Perot resonator. Pressure in Pa.~~..22

~~**Figure 8** : Pressure distribution along centerline of the 6.2 mm long Fabry-Pérot resonator, moving from the top (inside of the chamber) to the bottom (outside of the chamber).~~ 23

~~**Figure 9** : Plots representing the pressure field within the acoustic chamber designed to excite four resonators. All axes in units of Pascals. Plots (a), (b), and (c) show the acoustic pressure in the chamber on the bottom of the chamber (at the entrance of the resonators), halfway up the height of the acoustic chamber, and on the top surface of the acoustic chamber, respectively. Plot (d) shows the isosurface plot of the acoustic pressure within the chamber.~~ 24

~~**Figure 10** : Iso-surface plot of the total acoustic pressure within the air-filled chamber as solved by the finite element model.~~......................................25

~~**Figure 11** : FEM simulation of water-filled chamber during excitation by transducer located in the upper right corner of the chamber. The RMS acoustic pressure in Pascals is plotted. .....27~~

~~**Figure 12** : FEM model of the water-filled chamber. Isosurface plot showing the sound pressure in Pascals. .....27~~

~~**Figure 13** : Probe microphone in chamber on the left, including 3D-printed adapter (b) attached to ultrasonic transducer (a) and fused silica tubing (c) glued to the adapter. On the right, the tip of the probe inserted through the side of the chamber (d). .....30~~

~~**Figure 14** : Real color imagery of the luminol solution-filled chamber recorded during sonication, 5 minutes exposure time. (a) is the bounds of the chamber, (b) is the location of the transducer horn. .....31~~

~~**Figure 15** : Chamber used in first gel polymerization experiment. .....33~~

~~**Figure 16** : Chamber used in second gel polymerization experiment. .....33~~

~~**Figure 17** : Resonant chamber acoustic field comparative analysis. (a) Results of the FEM simulation of the air-filled acoustic chamber. The heatmap shows a regular pattern of pressure antinodes. The line plot below shows the pressure variation alongside a single edge of the vessel, displaying clearly peaks and troughs in the measurement. (b) RMS pressure measured with the probe microphone. The line plot below shows the pressure variation alongside a single edge of the vessel, displaying peaks and troughs in the measurement. (c) Mapping of the relative error between the empirical and experimental RMS pressure. Blue regions are where the simulated pressure was much lower than the experimental, red are where it was much higher, white are where it was within +/-50% of the value.~~

~~Many topological features are captured in both, including the pressure antinodes and the two hexagon-shaped features at 36 and 70 mm alongside the X axis. ....34~~

~~**Figure 18** : Validation of the numerical model of an ultrasonic sonoreactor with experimental results (Reproduced from (57), copyright 2020, Elsevier)36~~

~~**Figure 19** : Processed data output of SCL experiment. (b) shows the raw light information in monochrome. The red line represents the data plotted in (a) and the blue line represents the data plotted in (c). (d) shows the area of the graph where the luminosity recorded is more than 20% higher than the base luminosity recorded in the dark parts of the image (attributed to sensor noise). This area represents 1.707 cm^2. The "Light detected" axes in (a) and (b) range from 0 to 1, above which the camera sensor was overexposed. ....37~~

~~**Figure 20** : Images of hydrogels polymerized using ultrasound. (a) Set of three hydrogels polymerized in a closed vessel by applying an ultrasonic excitation for 5 minutes to a solution through the PET film at three points separated from each other by three centimeters. (b) Gel polymerized in a vessel through direct application of an ultrasonic excitation for 5 minutes. ....39~~

~~**[remove this]**~~

Commented [JL8]: Fix this

Formatted: Highlight

Formatted: Indent: Left: 0 cm, First line: 0 cm

List of Tables

Table 1: Summary of FEM models developed and simulated. 27

~~**Table 1**: Summary of FEM models developed and simulated. ....21~~

List of Abbreviations

SCL: Sonochemiluminescence

FEM: Finite Element Modeling

RMS: Root-Mean-Squared

OH: Hydroxyl Compound

Sono-RAFT: Sonochemically induced Reversible Addition-Fragmentation chain Transfer

PZT: Piezo Transducer

IDT: InterDigital Transducer

DG Methods: Discontinuous Galerkin Methods

SPL: Sound Power Level

Formatted: Indent: Left: 2 cm, Hanging: 1 cm, Don't adjust right indent when grid is defined

Formatted: Heading 2, Tab stops: Not at 16.49 cm

Formatted: Indent: Left: 0 cm, Hanging: 1 cm

Commented [JL9]: Must be more?

Formatted: English (Canada)

Contribution of Authors

In chapter 3 and 4, Louis-Jacques Bourdages and Jianyu Li conceived and designed the study. Louis-Jacques Bourdages performed the experiments and conducted the simulations. Louis-Jacques Bourdages and Jianyu Li analyzed the data and wrote the manuscript. Jianyu Li supervised the project.

Chapter 1. Introduction

1.1. Background

~~In recent years, there has been~~Recent years witnessed a growing interest in ~~the careful~~the engineering~~–~~ of acoustic fields, driven by the emergence of new applications that harness the unique properties and capabilities of resonant acoustic fields. Acoustic fields represent a promising method to interface with and manipulate materials, offering characteristics that set them apart from conventional processes. Notably, their ability to facilitate contactless interaction between the actuation source and the target material is unique and appealing, garnering ~~has garnered~~ significant attention (*1*). This attribute proves particularly advantageous, when seeking to apply effects through fluid volumes or impermeable membranes (*2*). For instance, the medical industry widely employs low-power ultrasonics for non-invasive scanning of the human body through echolocation, effectively penetrating the patient's skin and tissues.

While low-power soundwaves have found extensive use in medical imaging applications, where the pressure wave cause minimal disturbance and stress in the tissue (sound intensity of less than 1 W/cm^2 (*3*)) the ~~potential~~ application of higher power soundwaves (sound intensity of over 1 W/cm^2) is ~~an active field of study~~under active development. Harnessing higher power soundwaves presents challenges, including increased stresses and heat generation within the transmission material, but also opens up novel opportunities. One such exciting avenue is acoustophoretics, wherein localized areas of high acoustic pressure, in the range of hundreds to thousands of Pascals, are leveraged to exert forces on objects, enabling precise manipulation even at ~~the~~ microscales (*4*). Acoustophoretic techniques offer

Commented [JL10]: Provide a range to clarify what you meant by low and high power here.

Commented [LJ11R10]: Added range for low and high power.

Commented [JL12]: Value/range?

The order of 100 Pa?

Commented [LJ13R12]: Added value.

diverse possibilities across biology, chemistry, medicine, and various other disciplines, prominently featuring in lab-on-a-chip applications for droplet manipulation and an emerging application ~~o~~in~~f~~ bioprinting (*5*). Cell separation is another topic, this one in health sciences, where acoustophoresis has provided an effective solution to the long-standing problem of cell sorting (*6*, *7*).

However, despite remarkable progress in acoustophoretic applications, the majority of these efforts have been limited to two-dimensional fields, wherein the third dimension of the acoustic field is intentionally constrained. One reason is that t~~T~~ridimensional (3D) resonant acoustic fields present a more intricate analytical challenge and result in smaller acoustic forces, somewhat detracting from their widespread adoption, and being limited to acoustic tweezers for the most part (*8*). Nonetheless, ~~tridimensional~~ 3D resonant acoustic fields could enable novel additive manufacturing methods (*5*) and facilitate the manipulation of medical instruments and treatments within living organisms (*9*), among other notable applications.

Other domains of research related to engineered acoustic fields ~~have also been~~are also garnering increasing attention in the scientific community. Cavitation is one such application and is a process wherein a microscopic bubble will begin growing within a fluid put under low pressure (*10*) suddenly. These bubbles grow in a short timeframe which is correlated to the frequency of the event causing the change in pressure (in ultrasound, this may be as short as a microsecond, or even nanoseconds), and in the right conditions, such as the local pressure returning to a value much higher than the pressure within the bubble (as may happen if the bubble moves to another part of the fluid, or over the course of a sinusoidal pressure wave), may collapse. This collapse of the bubble leads to extremely high local temperatures and pressures (>3000K and >100 atm of pressure) at the point of implosion (*11*), and those extreme conditions have many implications. If cavitation happens

Commented [JL14]: Ref

Commented [LJ15R14]: Added reference

Commented [JL16]: Value,

Commented [LJ17R16]: Added values and explanation of correlation with pressure wave source frequency.

Commented [JL18]: Explain briefly what condition

Commented [LJ19R18]: Added explanation on conditions for bubble collapse.

Commented [JL20]: Again give some ranges.

Commented [LJ21R20]: Added values.

unintentionally, as in the low-pressure wake of a propeller or turbine, these bubbles cause intense wear and tear ~~due~~ through erosion (*12*). It is also a source of noise and ~~wastes a portion~~loss of some~~the~~ kinetic energy of the pressure wave traveling through the fluid through heat.

There are many systems where cavitation is beneficial and desired, however. ~~It is m~~Most commonly seen ~~in~~ are ultrasonic cleaning applications, where the wearing effect of the bubble implosion is used to dislodge impurities and fluid coatings from the surfaces of intricate objects (*13*, *14*). It is also employed to improve the dispersion and mixing of materials in lab~~oa~~ratory and industrial manufacturing settings. Moreover, the implosions of cavitation bubbles ~~have the property of synthesizing~~~~could~~ form OH radicals in aqueous solutions (*15*, *16*), offering pathways in a wide range of chemical reactions, known as sono~~-synthesis~~chemistry. In modern medicine, ablative cavitation has been employed for non-invasive surgical procedures, precisely targeting tissue destruction with focused soundwaves, obviating the need for incisions (*17*, *18*).

Despite these valuable applications, current uses of cavitation primarily involve undirected soundwaves or focused soundwaves facilitated by acoustic lenses. Only a limited number of applications capitalize on tridimensional pressure fields to pattern cavitation in accordance to an intricate motif. A patterned cavitation framework opens new possibilities, enabling macro-scale surgical treatments and increasing the throughput of sonochemical or material-mixing production lines. Thus, the exploration of tridimensional cavitation patterns holds the promise of driving advancements the field.

1.2. Thesis Structure

This thesis includes four chapters as follows. Chapter 1 introduces the background of the study~~study~~ and its structure. Chapter 2 reviews the current literature in the fields of ~~three dimensional~~3D acoustic fields and their analysis, acoustophoretics, cavitation and applications. Chapter 3 describes the design process and outputs of the FEM numerical models used in this project. Chapter 4 covers the work done to ~~analyze~~ measure the acoustic pressure field within a resonant chamber and comparisons to the numerical models, as well as sonochemiluminescent imagery of a resonant chamber with a corresponding simulation. Chapter 5 is the conclusion of this thesis and includes suggestions for future work in the field.

Chapter 2. Literature Review

Commented [JL22]: Present a figure showcasing the representative works related to this thesis, as people do for a review paper.

2.1. Acoustics

2.1.1. Introduction

~~With these motivation~~To assist in developing workflows able to engineer acoustic fields with specific desirable characteristics~~s~~, this ~~research project~~thesis aims to investigate the ~~the analysis of~~ tridimensional acoustic fields both computationally and ~~in practice and theoretically~~experimentally, as well as ~~–~~their potential applications. The first step is to gain an understanding of the linear acoustic fields, which drive the functioning of the phenomena of interest to us. A resonant acoustic field exhibits significant importance in this context. Resonant acoustic fields adhere to the principle of superposition (*19, 20*), wherein the total acoustic field resulting from the combination of multiple sources is equivalent to the sum of the individual fields generated by each source. This principle holds true when sound waves do not interact with each other in a nonlinear manner. Nonlinear interactions may occur when sound waves interact constructively with enough resulting amplitude to create a shock in the system, where such a discontinuity would result in a failure of the principle. The sound sources ~~of sound~~ in resonant acoustic fields encompass reflected, refracted, and transmitted waves. A resonant acoustic field, or standing wave, emerges as a consequence of a set of traveling soundwaves where points of maximal acoustic pressure, resulting from the superposition of the soundwaves, remain stationary relative to a designated reference point (*21, 22*).

Commented [JL23]: What motivations?

Commented [LJ24R23]: Added sentence for motivation

Commented [JL25]: More details, for instance, under what conditions the nonlinearity could merge and the principle fails.

Commented [LJ26R25]: Added example of when nonlinear interactions may occur.

A series of assumptions must be made to ensure the linearity of an acoustic field. First, the medium should be homogeneous and isotropic (*23-25*), meaning that the properties of the medium (e.g., density, speed of sound) do not vary significantly with position or direction. Second, linear equations will work best for single frequency or narrowband acoustic signals. If the sound field contains a wide range of frequencies, nonlinear interactions between different frequency components may arise (*26*), complicating the prediction using linear equations. Third, the amplitude of the sound wave should be relatively small compared to the ambient pressure of the medium. -High amplitudes can lead to shock formation and saturation effects (*27*) in the fluid, which are incompatible with the linear acoustic equations.

If those conditions are ensured, a tridimensional acoustic field can be simulated by solving the Euler Equation derived from the adiabatic equation of state: $\nabla^2 p - \frac{1}{c^2}\frac{\partial^2 p}{\partial t^2} = 0 \; (Eq. 1)$, where ∇^2 is the Laplace operator, p is the acoustic pressure, and c is the speed of sound in the medium. ~~[to solve it, what typically boundary and intital conditions, what solver?]~~To solve this equation, we use FEM using a method in the Runge-Kutta family, with boundary conditions typically defining the boundaries of the domain in which soundwaves are being simulated. An example of this ~~This type of~~ analysis is found in existing literature. ~~(Figure~~ Figure 1~~1)~~ (*28*) shows a comparison between the raw sound pressure data measured in a water-filled vessel on the left, and a corresponding FEM model based on a solution of the Euler equation. Note the peaks in pressure in the center of both datasets, which is the point below the transducer.~~[add a few sentences to explain the follow figure, what is the results about ?????]~~

In applications involving acoustophoretics and cavitation, these conditions are rarely met, and corrections must be applied to obtain an accurate simulation. The Westervelt equation, a fundamental partial differential equation, can be used to describe the propagation of nonlinear acoustic waves in a fluid medium (*29*). It takes the following form: $\frac{1}{\rho c^2}\frac{\partial^2 p}{\partial t^2} + \nabla\left(-\frac{1}{\rho}\nabla p - \frac{\delta}{\rho c^2}\frac{\partial \nabla p}{\partial t}\right) = \frac{\beta}{\rho^2 c^4}\frac{\partial^2 p^2}{\partial t^2} \; (Eq. 2)$, where β is defined as the coefficient of nonlinearity, and δ the diffusivity of sound.

Formatted: Font: Not Bold

Field Code Changed

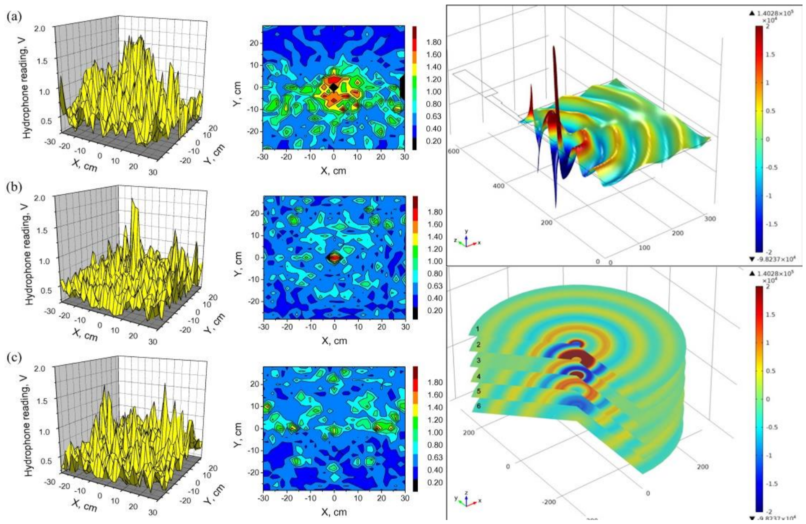

***Figure 1** : Experiment comparing numerically simulated and empirical acoustic fields. Mapping of hydrophone measurements in plexiglass water-filled tanks at three different heights (a, b, c) (left) and simulation of acoustic pressure distribution within tank (right). (Reproduced from (28), copyright 2016, Elsevier)*

~~In applications involving acoustophoretics and cavitation, these conditions are rarely met, and corrections must be applied to obtain an accurate simulation. The Westervelt equation, a fundamental partial differential equation, can be used to describe the propagation of nonlinear acoustic waves in a fluid medium~~ (*29*)~~. It takes the following form:~~ $\cancel{\frac{1}{\rho c^2}\frac{\partial^2 p}{\partial t^2} + \nabla\left(-\frac{1}{\rho}\nabla p - \frac{\delta}{\rho c^2}\frac{\partial \nabla p}{\partial t}\right) = \frac{\beta}{\rho^2 c^4}\frac{\partial^2 p^2}{\partial t^2}}$ ~~,.~~ ~~where~~With ~~β~~ is ~~defined as the coefficient of nonlinearity, and δ defined as the diffusivity of sound.~~ The diffusivity of sound depends on the physical properties of the medium, such as its shear and bulk viscosity, t~~its t~~hermal conductivity and the~~its~~ specific heat at constant volume and pressure. This term ~~for~~ represents the energy dissipation into the medium as the wave travels (essentially friction losses between the moving air particles as they are agitated through the medium), while the coefficient of nonlinearity captures the effects of the interactions between the high-energy waves,

Formatted: Centered

Commented [JL27]: What you mean

Commented [LJ28R27]: Added explanation that those losses are comparable to friction losses.

which ~~lead to~~result in an intrinsic deformation in the traveling waves, leading for example to a sinusoidal wave shifting to a sawtooth-shaped wave due to the pressure peaks of the wave traveling faster than its troughs (*30*).

The Westervelt nonlinear equation allows for the accurate simulation of higher amplitude resonant acoustic fields.~~,~~ H~~h~~owever, ~~note that~~it should be noted that it does not account for the effects of cavitation on the sound field, only of effects where the medium remains in a single phase.

2.2. Acoustophoretics

2.2.1. Introduction

With a simulation of the acoustic field, one can predict the sound pressure at every point in the medium ~~can be predicted~~. This is the measure of greatest importance for acoustophoretics. Indeed, the acoustophoretic force arises when the surface of the object is subjected to a varying pressure field. The magnitude of this force depends on the sound radiation pressure on the object. Sound radiation pressure is a nonlinear phenomenon (*31*) that occurs when sound waves exert a force on a surface due to the transfer of acoustic energy (*31*). When a sound wave propagates through a medium, it generates variations in air pressure that result in mechanical vibrations in objects. This transfer of acoustic energy manifests as the sound radiation pressure.

In a resonant acoustic chamber, this pressure field will take the form of a standing wave, which consists of a set of pressure nodes and antinodes where the periodic variation in pressure will be zero and maximized, respectively. The spacing between the nodes ~~will~~ depends on the wavelength of the sound source exciting the chamber, which results in higher frequency sounds creating a greater number of periodically located pressure nodes.

The nonlinear effect of sound attenuation becomes increasingly important at the high frequencies used in applications related to acoustophoretics and cavitation. The decay rate due to thermoviscous losses is found to increase quadratically with the angular frequency of the sound (*32*). This higher decay rate ~~rate leads to a restriction on the~~has an effect on the size of resonant chambers (*33*) that may be used with very high frequency sound sources~~,~~. Achieving resonance with low frequency sound in a large room can be done, but for ultrasound, the decay of the traveling soundwave can dampen resonance in larger spaces~~and must be accounted for in their design~~.

2.2.2. Applications of Acoustophoretics

~~Today, t~~The most common application of acoustophoretics is in particle or droplet manipulation in lab-on-a-chip systems. These systems offer many advantages, the foremost of which being the ability to process minuscule amounts of reagent, leading to reduced waste of material, accelerated reactions, and lower requirements of sample (*34, 35*). This can be achieved by replacing a wide range bulkier instruments designed to manipulate and measure out quantities of fluid with acoustic tweezers (~~Figure~~ Figure 2~~2~~) (*36*), which make use of carefully positioned antinodes of pressure to apply acoustophoretic forces as required to move droplets from one step of a given protocol to the next. These have found great usefulness in experiments involving sub-millimeter objects, including single-cell manipulation, cell separation and trapping, or nanomaterial manipulation (*37*).

Commented [JL29]: Rephrase

Commented [LJ30R29]: Rephrased for clarity

Formatted: Font: Not Bold

Field Code Changed

Formatted: English (Canada)

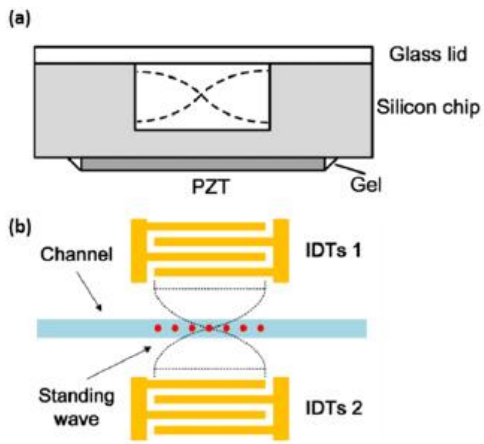

***Figure 2** : Acoustic tweezer designs. Schematic of acoustic manipulation device based on Bulk Acoustic Waves (a) and Surface Acoustic Waves (b) (Reproduced from (36), copyright 2019, IOP Publishing)*

Lab-on-a-chip methods have involved two-dimensional acoustic fields, but more recent investigations into applications of acoustophoretics have made use of three-dimensional acoustic fields. Foresti et al. developed an apparatus to achieve droplet separation at a smaller radius through the use of acoustophoretic forces. This type of droplet separation has uses in bioprinting applications (Figure 3) (*5*). To achieve this, a particular type of resonator is used. The Fabry-Perot resonator (*38*, *39*) is a cavity made of two parallel reflecting surfaces, which can be achieved with two parallel planes, or with a cylinder. Its principle can be applied to both electromagnetic wave and sound waves.

Formatted: Font: Not Bold

Commented [JL31]: Rephrase

Commented [LJ32R31]: Elaborated and clarified.

~~Lab-on-a-chip methods have involved two-dimensional acoustic fields, but more recent investigations into applications of acoustophoretics have made use of three-dimensional acoustic fields. Foresti et al. developed an apparatus to achieve droplet separation at a smaller radius through the use of acoustophoretic forces. This type of droplet separation has uses in bioprinting applications (Figure 3) (5). To achieve this,~~

~~a particular type of resonator is used. The Fabry-Perot resonator~~ (*38, 39*) ~~is in both optics and acoustics a cavity made of two parallel reflecting surfaces, including cylinders.~~ With the right dimensions, this resonator can act as a band-pass filter tuned to a frequency range dependent on the physical dimensions of the device. These dimensions are found to correspond to $Height = 0.36\lambda$, $Diameter = 0.14\lambda$ $(Eq. 3)$ for a cylindrical cavity filled with air, where λ is the wavelength (*39*). Note that these dimensions depend solely on wavelength, and thus the speed of sound in the medium and frequency of the soundwave. These values correspond to the first Fabry-Pérot resonance, for a given wavelength there also exist additional resonances at higher harmonics~~-~~ where the height of the resonator could be increased.

Within the subwavelength cavity, resonance is achieved for waves of the right frequency, leading to high acoustic pressures. These high acoustic pressures, and thus high-pressure gradients, can be used to apply an acoustophoretic force to a droplet suspended from a nozzle located in the cavity. This method has many advantages compared to other ways to separate droplets. Relying on gravity results in larger droplets, since the force pulling the droplet downwards is proportional to its mass and cannot be increased further.

Commented [JL33]: Rephrase

Commented [LJ34R33]: Elaborated and clarified.

Commented [JL35]: Do the numbers depend on the medium property?

Discuss briefly on the numbers

Commented [LJ36R35]: Mentioned medium properties and the dependence of the number on the fabry-perot resonance in use.

Formatted: Line spacing: 1.5 lines

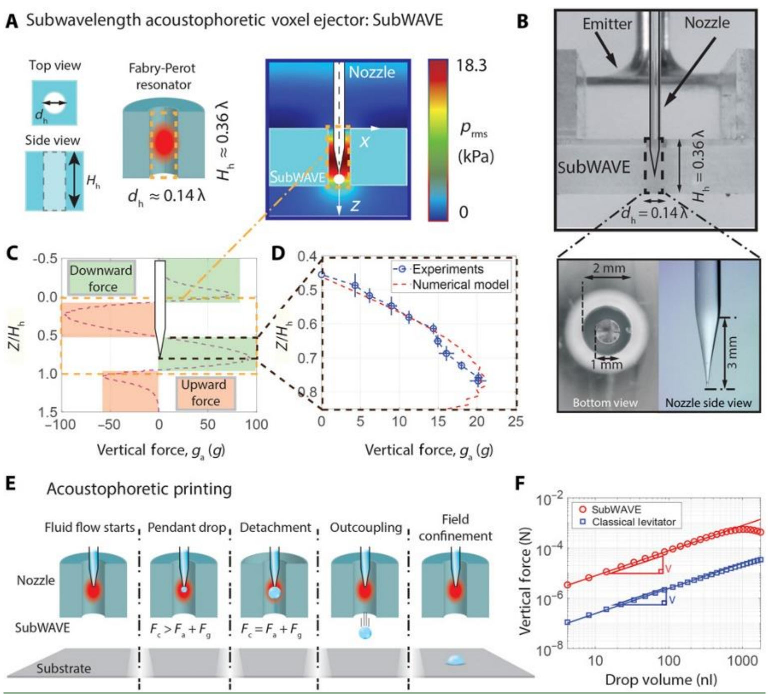

***Figure 3** : Principle and acoustophoretic properties of the subwavelength resonator. (A) Schematic view of the subwavelength acoustophoretic voxel ejector (left). The resonance (schematically shown in red) leads to high acoustic pressure amplification while keeping the field strongly confined (right). (B) Side view of the experimental setup (top) and close-up of the tapered nozzle (λ ≈ 14 mm) (bottom). Calculated vertical force distribution inside the subWAVE (C) and its experimental validation (D). (E) Schematic illustration of acoustophoretic printing. (F) Log-log plot of vertical force generated within the subWAVE as a function of drop volume compared to a classical standing-wave levitator. (Reproduced from (5), copyright 2018, AAAS). ~~ABCEDF~~*

~~Within the subwavelength cavity, resonance is achieved for waves of the right frequency, leading to high acoustic pressures. These high acoustic pressures, and thus high pressure gradients, can be used to apply an acoustophoretic force to a droplet suspended from a nozzle located in the cavity. This method has many advantages compared to other ways to separate the droplet~~s~~. Relying on gravity~~

Formatted: Centered

Commented [JL37]: For all figures, you should clarify ABCEDF even those you cited for readerability.

Correct this caption and others

Commented [LJ38R37]: Corrected caption

~~results in larger droplets, since the force pulling the droplet downwards is proportional to its mass, and cannot be increased further.~~ Using electrical or magnetic forces requires specific material properties from the ink (*40*), either the ability to be charged, or displaying ferromagnetism. Other techniques, like inkjet printing, demand specific mechanical properties from the ink, such as low viscosity (*41*). Acoustophoretic forces can achieve droplet separation while accommodating a wider range of materials.

Commented [JL39]: Remove the kind of big white space

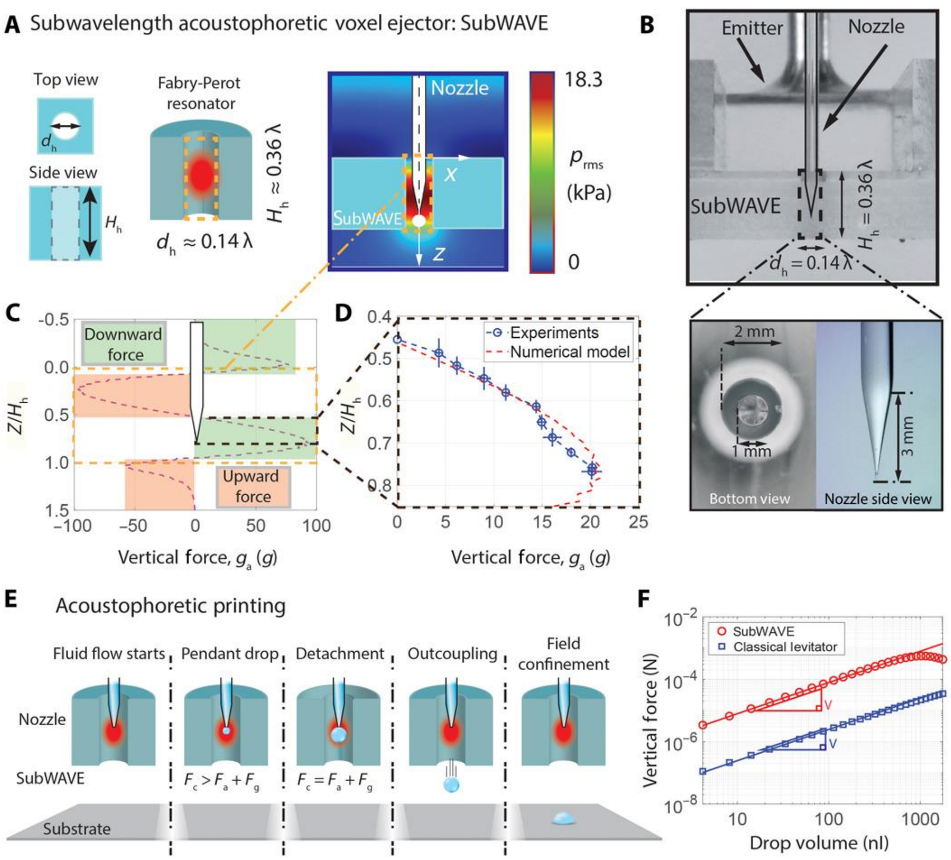

~~**Figure 3** : Principle and acoustophoretic properties of the subwavelength resonator. (Reproduced from (5), copyright 2018, AAAS)~~

Formatted: Normal

2.3. Cavitation

2.3.1. Introduction

~~An important research question regards the~~The relation between the ~~afore-mentioned~~ pressure antinodes and the inception of cavitation bubbles is a critical element of this study. The first condition for cavitation to occur is that the local

Commented [JL40]: Rephrase

Commented [LJ41R40]: Rephrased

pressure must fall below the vapor pressure (*10*) of the fluid, resulting in the fluid being forced to a gaseous phase of its phase diagram (*10*). The second condition is that nucleation must occur. Nucleation may occur on surface irregularities on the container filled with the fluid, or it may happen on microscopic particles in suspension in the fluid. This is similar to the bubble nucleation in a boiling liquid. Once nucleation begins, the vapor cavity oscillates with the sound wave, growing in size until it reaches a critical size. At this critical size, the bubble may begin collapsing under the pressure of the rest of the fluid. This implosion generates high temperatures (>2000 K) (*42*) and pressures of hundreds of atmospheres (~~xxx~~>100 MPa) (*43*). Some light is also generated due to the high temperature of the vapor, a phenomenon called sonoluminescence. After this extreme event, the vapor bubble may rebound and regrow into a new cavitation bubble, or dissipate entirely.

Commented [JL42]: Add

Commented [LJ43R42]: Added value.

Besides the nature of the fluid, two other parameters are ~~of particular import~~important to the characteristics of the cavitation bubbles. The amplitude of the soundwave has the straightforward effect of increasing the size and quantity of the cavitation bubbles (*44*), as a greater amplitude results in more of the fluid being brought below the vapor pressure of the medium. ~~The second parameter is the frequency of the sound exciting the fluid. Increasing this frequency leads to generally smaller bubbles, and is associated with a higher production of OH radicals (Figure 4)~~ (*15*, *43*, *45*)~~ up to around 500 kHz. Large bubbles clouds are associated with the disruption of the transmission of sound through fluid~~ (*46*)~~, which would impede the formation of a standing wave in an acoustic chamber, so an aim of this research will be to verify whether cavitation induced with lower frequency ultrasound (~20 kHz) prevents resonance within a purpose-designed chamber.~~

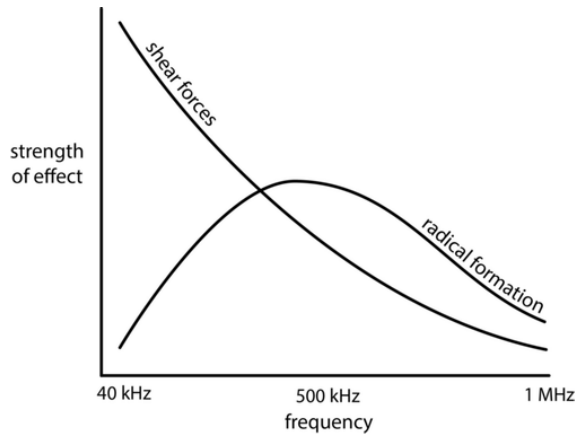

***Figure 4** : Generalized profiles for the strength of effects correlated to the mechanical shear forces generated from the collapsing bubble, and the reactive radicals formed from vapor molecule sonolysis. (Reproduced from (45), copyright 2019, Wiley-VCH)*

The second parameter is the frequency of the sound exciting the fluid. Increasing this frequency leads to generally smaller bubbles, and is associated with a higher production of OH radicals up to around 500 kHz (Figure 4) (*15*, *43*, *45*) ~~up to around 500 kHz~~. Large bubble~~s~~ clouds are associated with the disruption of the transmission of sound through fluid (*46*), which would impede the formation of a standing wave in an acoustic chamber.~~,~~ ~~S~~so ~~an aim of this research will be t~~it remains~~ing~~ unclear ~~o verify~~ whether cavitation induced with lower frequency ultrasound (~20 kHz) prevents resonance within a purpose-designed chamber.

Formatted: Normal

Formatted: Font: Not Bold

Field Code Changed

2.3.2. Applications of Cavitation

Cavitation has a wide range of applications, including cleaning and fluid homogenization. The use of sonochemistry for the activation of polymerization reactions has been garnering interest as this method has the potential to enable more precise control of polymer chain lengths and molecular weight distributions (*45*), to minimize and even avoid the use of radical initiators, and also allow for the polymerization of gels hidden behind opaque materials, which would prevent the use of the more widespread light-activated polymerization (*47*).

This type of polymerization relies on the radical-synthesis properties of the cavitation bubbles. These OH radicals are created when the extreme conditions in and around the bubble cleave the water molecules, leaving the highly reactive hydroxyl compounds. Then, the hydroxyl may act as the initiator for the radical polymerization of a compound using monomers dissolved in the solution. An example of such a reaction is sonochemically induced reversible addition-fragmentation chain transfer polymerization, or Sono-RAFT polymerization. The reaction and excitation methodology of this process is summarized in ~~(Figure~~ Figure 5~~5)~~ (*45*). The progress of the reaction is also quantified by correlating the conversion fraction of monomer to polymer and the average molecular weight of the end product. The gels produced with this method can show tough hydrogel mechanical characteristics, and can undergo further crosslinking processes (*48*) for further improved properties.

Commented [JL44]: Ref?

Commented [LJ45R44]: Added reference

Formatted: Font: Not Bold

Field Code Changed

Commented [JL46]: Has any prior work showed this point?

Commented [LJ47R46]: This is a result from Yixun's experiments. Double network PEGDA/Chitosan hydrogels.

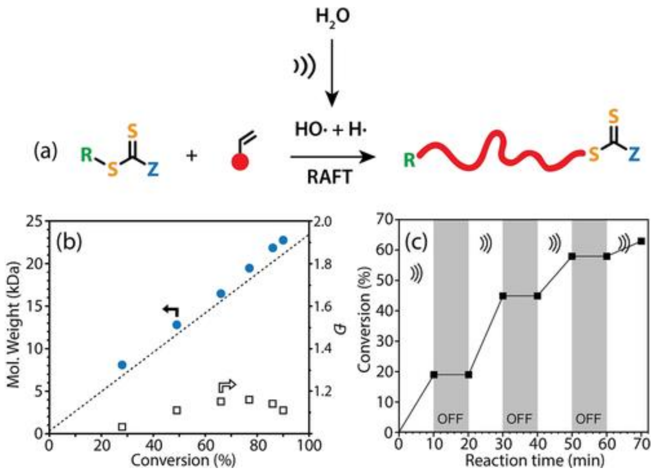

***Figure 5** : Hydrogel polymerization reaction summary. Scheme for Sono-RAFT polymerization (a). Molecular weight evolution characteristics with regards to monomer conversion during Sono-RAFT polymerization (b). Protocol to complete the monomer conversion with periods of ultrasonic excitation denoted with a symbol and periods of pause excitation in grey (c). (Reproduced from (45), copyright 2019, Wiley-VCH)* ~~(c) is missing~~

2.4. Finite Element Modeling

2.4.1. Introduction

Partial differential equation-based problems such as the ones used to solve for the nonlinear acoustic behaviours of this study are often tackled with numerical methods, specifically Finite Element Modeling (FEM). This is because the empirical systems of interest have a level of complexity which would be difficult or impossible to represent with an analytical solution. For this purpose, the COMSOL Multiphysics software is used to create models which will be validated against the experimental results of corresponding physical systems. These models will use the Westervelt equation as laid out previously, in Eq. 2 in Section 2.1.1. The walls of the acoustic chambers are assumed to be rigid, which is a satisfactory approximation for the hard

Commented [JL48]: Add more details and review the methods in the FEM used later.

Commented [LJ49R48]: Added more review and information on the methods used in the FEM models.

Commented [JL50]: Where?

Commented [LJ51R50]: Added direct reference to relevant equation and section acrylic walls, leading to the use of a reflecting boundary conditions for those surfaces. The open air on the other hand is approximated with a non-reflecting boundary condition located a distance of a few wavelengths away from the openings of the chambers, which is a sufficient approximation due to the high decay rate of the high frequency sound (*49*). Finally, the sound source is approximated by using a surface oscillating alongside its normal direction with a frequency and amplitude matching that of the ultrasonic transducer used in the empirical setup.

The specific technique used to solve the differential equations corresponding to nonlinear acoustics in the COMSOL engine is the D~~d~~iscontinuous Galerkin (DG) method (*50*). This family of methods has characteristics which make them ideally suited to this type of application.

Commented [JL52]: Add a few sentences to explain this method.

Commented [LJ53R52]: Added more information on DG methods

First, they are locally conservative, meaning models correctly described by local mass conservation can be used effectively with the technique. This property is due to the fact the method enforces the system equations element-per-element over the mesh studied. Said mesh can have elements of varying sizes and complex topology, which is useful in adaptive strategies and for multi-physics problems.

A second important property is that they are high-order accurate. This is especially useful to maintain an accurate solution around shocks and other discontinuities.

Thirdly, a considerable advantage of DG methods is that they produce mass matrices which are block-diagonal in mass transfer problems, allowing for high parallelizability and thus improved computational performance (*51*).

To generate the dimensions of the acoustic chambers, a numerical optimization method is used. A gradient-free optimization algorithm is used to vary a set of design parameters within a design space. These algorithms are used when the objective function of a problem is unknown or incompletely known, and are designed to

Commented [JL54]: Have you illustrate these details somewhere? You need to show them in the Chapter 3.

Commented [LJ55R54]: The optimization parameters (chamber dimensions, transducer locations) are laid out in Section 3.1.

converge towards a solution in as few steps as possible, since these "Black Box" functions are often expensive and slow to compute. They operate by evaluating the system while varying the parameters, which provides information on the potential trends and correlations found within. These trends can be followed to arrive to an optimize solution. Some algorithms implement features to avoid missing a global optima due to the presence of a local optima, such as basin-hopping (*52*).

A few factors influence the performance of such optimization algorithms. The number of dimensions of the problem, or the number of its variables increases the search space exponentially. The presence of many local maxima and minima due to a noisier function can also make the search more difficult. Due to those factors, it is best to design the problem so as to minimize the number of variables, and to reduce the coupling of the variable, so that the algorithm may optimize them independently.

Constraining the optimization parameters to a specific range can also help accelerate the search by preventing the evaluation of unphysical models, or it can allow the optimization to take into account manufacturing limitations that would exist in the real-world system.

For the systems investigated in this work, the Nelder-Mead algorithm (*53*, *54*) is used. An implementation of this algorithm is provided in the Optimization module of the COMSOL program, allowing for connection the input parameters and output solutions of the FEM models to the search of the optimization algorithm seamlessly. It is a direct search method and is useful to minimize or maximize functions in a multidimensional space where derivatives may not be known, as is the case in FEM simulations of a nonlinear acoustic system. It works by creating a simplex in the design space (for example, a triangle of three points with differing parameters in a system with two parameters, or a tetrahedron in a design space with three dimensions). This simplex is then manipulated by moving one of the vertices in the

Commented [JL56]: Exactly how to optimize?

Commented [JL57R56]: Optimization constraints…

Commented [JL58R56]: You don't discuss your results here. But you need to review those methods will be used later

Commented [LJ59R56]: Explained the idea of numerical optimization, and the use of constraints.

Commented [JL60]: Explain.

Commented [LJ61R60]: Explained how the Nelder-Mead algorithm is interfaced with in comsol and how it interacts with the model.

Commented [JL62]: Breifly introduce this

Commented [JL63R62]: What specific FEM method you use here.

Commented [LJ64R62]: Added the discontinuous Galerkin method design space, by either expanding the simplex or contracting it, depending on which makes the search approach an optima. These manipulations of the simplex continue until its vertices have converged around an optima and are all within an arbitrary distance in the design space from one another (*55*). The Nelder-Mead method has been used to optimize the parameters of systems in material science where a large design space with multiple variables made more naïve search methods less effective. For example, composite structures with a complex geometry and multiple layers have made use of the method to find global optima for given requirements in Ghiasi et al.'s work (*56*).

Chapter 3. Finite Element Modeling for the Analysis of Ultrasonic Acoustic Fields

This chapter aims to answer the following questions: can COMSOL FEM-based models simulate subwavelength acoustic structures? Can the acoustic characteristics of multiple pressure antinodes be optimized at the same time? To what extent are the tridimensional acoustic fields computed with these methods accurate? And finally, what is the acoustic field computed by a single phase model for a system where cavitation will be expected?

To find those answers, a set of FEM models were used. The first two models investigated subwavelength resonators in air, at first a single resonator to verify the presence of subwavelength resonance in the results, and second an array of resonators to optimize a more complex acoustic field. The third model provided the theoretical data against which a set of empirical measurements were compared in Chapter 4. This allowed us to quantify the real-world accuracy of the simulation. The fourth and last model, using water, was also used as a point of comparison in Chapter 4 to determine the effects of cavitation on the development of the resonant standing wave.~~[Introduce your research plan in this chapter. Provide a rationale of your work in this chapter. What are the questions and objectives you want to address in this chapter? How is this chapter related to other chapters for cohesion of the cohesion of the thesis.]~~

~~[below you show models for water versus air, one resonator versus four resonators, so here you need to provide a rationale for why doing so.]~~

3.1. Numerical Models Setup

This project began~~ins~~ with a set of Finite Element Models (FEM) meant to simulate the conditions within acoustic chambers excited by an ultrasonic transducer. The

Formatted: Not Highlight

Formatted: Not Highlight

Formatted: Not Highlight

Formatted: Not Highlight

Formatted: Not Highlight

Formatted: Not Highlight

Formatted: Not Highlight

Formatted: Not Highlight

Formatted: Not Highlight

Formatted: Not Highlight

Formatted: Highlight

Formatted: Normal

ultrasonic transducer used is a piezoelectric transducer-based homogenizer equipped with a 3/8” titanium horn (VWR, 76193-588) and designed to be agitated by a 20 kHz sinusoidal wave. Its functioning frequency wa~~i~~s measured to be 19850 Hz with a microphone. This was done using the Spectroid Audio Spectrum Analyzer application and a standard phone microphone. This software provides a spectrum of the sound signal recorded by the device and provides a spectrum of the soundwave detected as the amplitude as a function of frequency. This spectrum showed a strong and narrow peak at 19850 Hz with a limited signal on the rest of the bandwidth, providing the frequency of the transducer. The amplitude of the transducer’s soundwave wa~~i~~s then measured at a set distance, and this amplitude wa~~i~~s used to adjust the amplitude and sound power level of the transducer used in the simulation.

The goal of the models was to investigate the design of an ultrasonic acoustic chamber through multiple approaches.

~~Four~~ Three models using air as the working medium we~~a~~re created. Air is used for two reasons. First, a probe microphone for recording sound in air can easily be assembled using readily available instrumentation. Second, there exists data for Fabry-Pérot resonators excited in air against which our work may be compared. ~~One~~ The first model wa~~i~~s designed to verify whether the ~~simulation~~ system ~~is able to could~~ could simulate subwavelength acoustic structures, such as those found in the Fabry-Perot resonator discussed in ~~the literature review~~a previous work (*5*). Its acoustic field ~~will~~ were then ~~be~~ compared to the results found in literature. The dimensions of the Fabry-Perot cylindrical resonator ~~will~~ followed the proportions laid out previously (See Section 2.2.2., Eq. 3), resulting in a diameter of 2.4 mm and a length of 6.1 mm. ~~The resonator wasis fabricated with a borosilicate capillary glued into a hole in the bottom of the acoustic chamber to be shown in Chapter 4.~~ The second model ~~will~~ wa~~i~~s to study the design process involved in the engineering of

Commented [JL65]: Have you anywhere the experiment and approach to measure and calibrate the frequency?

Please add. I rememberred you show me this data

Commented [LJ66R65]: Briefly explained how the spectrum analyzer is used and how the value for the frequency is obtained.

Commented [JL67]: First, provide a brief introduction of the four models. Why four? Again what differences?

Commented [JL68R67]: To clearly show the difference and details, you can list a table to list the key specifications.

Commented [JL69R67]: You simulated air and water in the chambers. You need to explain why so.

Commented [LJ70R67]: Added a few sentences to introduce the models and explain the choice of medium, added a table summarizing the characteristics of each chamber.

Commented [JL71]: What previously?

Commented [LJ72R71]: Added reference to relevant equation.

Commented [JL73]: You showed in chapter 4?

Commented [LJ74R73]: No, this was accidentally included. Removed.

acoustic fields with multiple periodic antinodes. This model ~~will~~ included four resonators arranged in a ~~square array~~rectangular array and excited with a single transducer. The location of the transducers and that of the pressure antinodes ~~will be~~were optimized jointly to obtain equal resonance in all four resonators. The arrangement of this array of resonators can be seen in ~~Figure~~ Figure 6~~6~~. Laying out resonators in a periodic pattern allows for an increase in throughput from the device, and this technique can be used to increase the productivity of other devices making use of pressure antinodes. The third model ~~i~~was designed ~~to function with air as a working fluid and is used~~ to validate the accuracy of the patterned pressure antinodes calculated by the simulation. The fourth and last model wa~~i~~s designed with water as the working fluid and ~~will be~~was used to verify the disruptive effect of cavitation on the formation of the standing wave. Water was used here, because a liquid medium is needed to demonstrate cavitation. See Table 1 for a summary of the acoustic chambers used in this thesis.

Commented [JL75]: Again you provide a rationale why four resonators? Is it that you want to do higher throughput?

Commented [LJ76R75]: Yes, added more detail.

Commented [JL77]: Make sure all figures are properly referenced.

Commented [LJ78R77]: Figure 6 shows a schematic of the system with four resonators

Formatted: Font: Not Bold

Formatted: Font: 7 pt

Commented [JL79]: Why doing water here?

Commented [JL80R79]: Current version is confusing and unclear to the readers why you do such four models.

Commented [LJ81R79]: Added explanation above on why air is used for the first three models and water for the fourth.

Formatted: Font: Not Bold

Formatted: Line spacing: Multiple 1.15 li

Formatted: Font: 7 pt

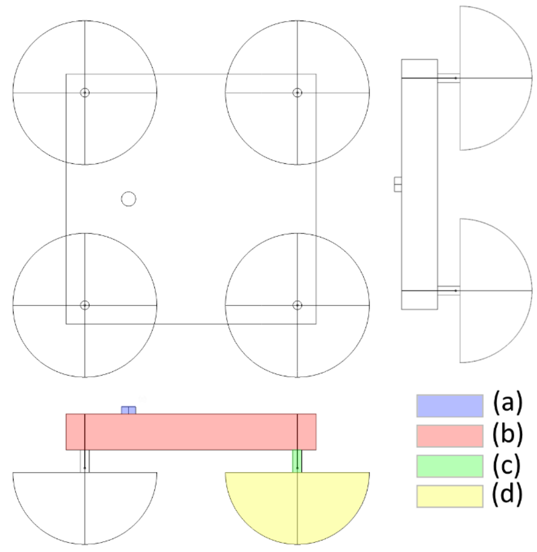
(a)
(b)
(c)
(d)

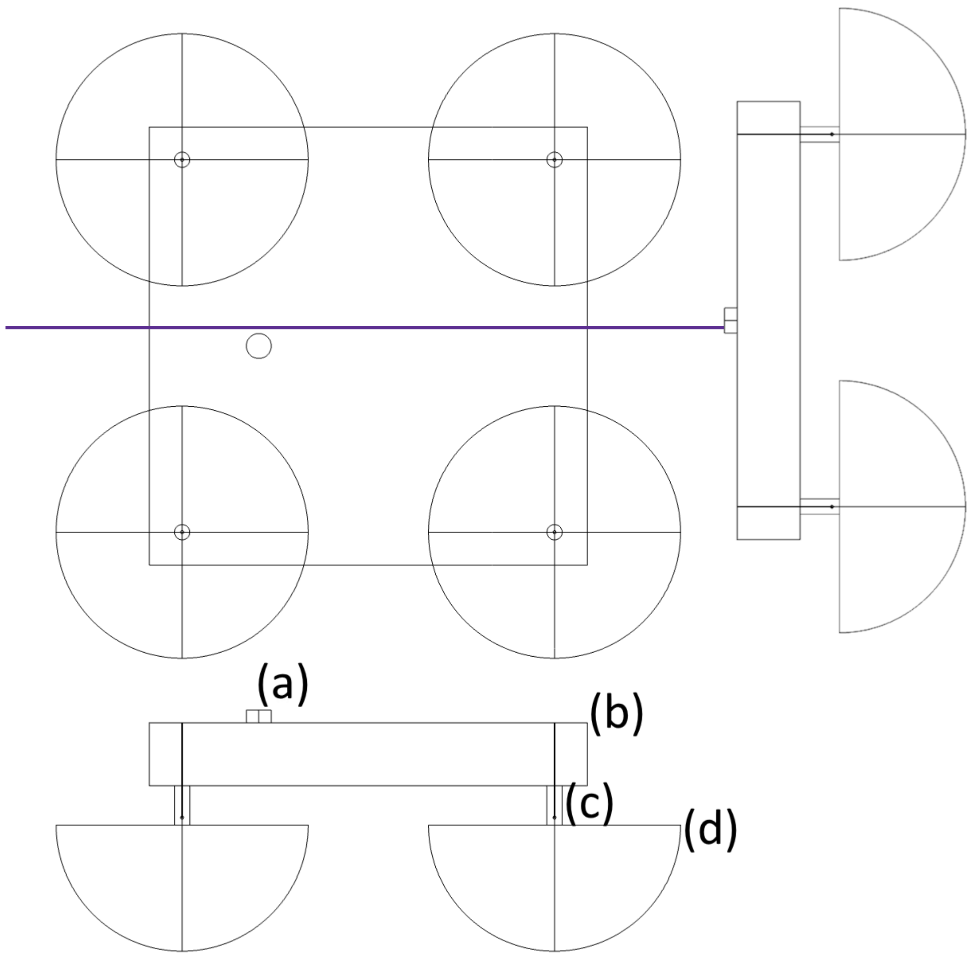

Figure 6 *: Schematic for chamber designed to excite an array of four Fabry-Pérot resonators. Note the location of the cylindrical ultrasonic transducer exciting the chamber (a), the extents of the acoustic chamber (a rectangular box) (b), the four cylindrical– resonators (c) and the four corresponding surfaces used for the calculation of the far field absorption of the sound waves emitted, which are modeled as hemispheres. The hemispheres are modeled to provide enough space for the soundwave exiting the aperture to develop fully, which improves the accuracy of the far field absorption (d) See Figure 9 for a 3D view of the system.*

Formatted: Centered, Don't keep with next

Commented [JL82]: Revise it, confusing, what area of abcd

Commented [LJ83R82]: Using colors to denote areas instead

Commented [JL84R82]: A, B top and side view.

The models we~~a~~re meshed with tetrahedral elements of a size smaller than a twentieth of the wavelength in size, which allow~~s~~ed the simulation to capture the details of the acoustic field fully (*57*, *58*). The wavelength depends on the frequency and speed of sound in the medium, so the element size ~~will be~~is different between the air-based systems and the water-based systems. The system studying the subwavelength structure ~~will~~ used even smaller elements for that region of the simulation, down to one hundredth the wavelength.

Commented [JL85]: Again, list a table to show the specifications of the four models. What is the exact element size for water and air model?

Commented [LJ86R85]: Added element size column to summary table.

For the air-filled chambers, standard air at atmospheric pressure and temperature (1 atm, 300K) wa~~i~~s used. For the water-filled chamber, although a luminol solution ~~will be used~~was used in the experiment, the physical properties of the solution relevant to the simulation are the same as for water.

Table 1*: Summary of FEM models developed and simulated.*

ACOUSTIC CHAMBER	**PROBE MICROPHONE**	**MEDIUM**	**RESONATORS**	**ELEMENT SIZE**
A	No	Air	Single	0.1 to 0.8 mm
B	No	Air	Array of four	0.1 to 0.8 mm
C	Yes	Air	None	0.8 mm
D	No	Luminol-water solution	None	2 mm

~~[Table to list the key modeling specification of the four models]~~

The Nonlinear Pressure Acoustics COMSOL module in the time explicit domain ~~are~~ we~~as~~re used, ~~to~~ where ~~include~~ the nonlinear components of the simulation were~~as~~ included through the Westervelt equation, as discussed in the background section. Then, the simulation wa~~i~~s computed until the system reached~~s~~ a steady state, after

0.01 seconds of excitation (~200 oscillations of the transducer). With these results, the acoustic pressure at points of interest can be obtained and compared against the empirical data that was gathered with the experiments in Section 4.2.1.

The optimizations of the acoustic chambers we~~a~~re conducted on a maximum of six parameters: the width, length and height of the chamber, the position of the transducer alongside the length and width of the top of the chamber, and the position of the resonator within the chamber. The acoustic chambers with Fabry-Perot resonators, chamber A and B, ~~systems~~ mad~~k~~e~~s~~ use of all variables, while the other two, chambers C and D, ~~experiments~~ mad~~k~~e use of only the first five. To obtain parameter values, the Nelder-Mead algorithm iteratively explore~~s~~d the design space using the simplex-based method explained in Section 2.4.1., seeking the optimal combination of parameters that yield~~s~~ed the highest pressure at the bottom of the chamber for ~~the two latter chambers~~chamber C and D, or the highest pressure within the resonator for ~~that system~~chambers A and B. This iterative process continue~~s~~d until the algorithm converge~~s~~d to a solution that maximized~~s~~ the desired pressure measurement. The convergence criteri~~a~~on is defined in the algorithm by a value of 0.0001 for the optimality tolerance. This value means that improvements over the current best solution cannot be found with steps in the scaled control variables (those variables being the dimensions of the chambers defined above) of relative size greater than this optimality tolerance.

Commented [JL87]: What empirical data?

Commented [LJ88R87]: Added reference to relevant section.

Commented [JL89]: What experiments? To be specific

Commented [LJ90R89]: Specified which chambers are being discussed.

Commented [JL91]: How to iteratively? Clarify the methodology of iteration.

Commented [LJ92R91]: Expanded on the iteration methodology in literature review and referenced here.

Commented [JL93]: What chambers? Please clarify

Commented [LJ94R93]: Clarified which chamber is being referred to.

Commented [JL95]: Methodology about the iterative process?

Commented [LJ96R95]: Expanded on the iteration methodology in literature review and referenced here.

Commented [JL97]: Clarify the meaning of this value?

3.2. Results and Discussion

3.2.1. Fabry-Perot Resonator Simulation

For this model, the Nelder-Mead algorithm ~~goes~~ went through ~~ninety six~~ninety-six evaluations of the system to stabilize to a system where the resonator wa~~i~~s excited effectively.

The solution of the system displays a series of six pressure antinodes located in a periodic pattern on the surface of the chamber.

~~The solution of the system displays a series of six pressure antinodes located in a periodic pattern on the surface of the chamber.~~

~~The Fabry-Perot resonator simulation (Figure 6) shows a region of higher acoustic pressure forms within the resonator, as predicted. The acoustic pressure is highest in the center of the resonator, and tapers to a low value towards the two ends of the cylinder, resulting in a strong pressure gradient which can be used to exert an acoustophoretic force.~~

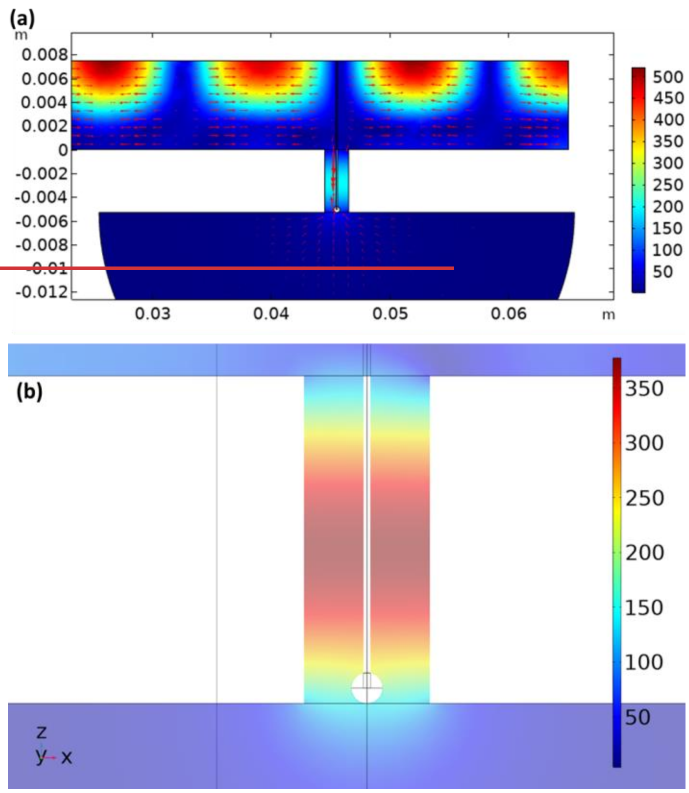
(a)
m
0.008
0.006
0.004
0.002
0
-0.002
-0.004
-0.006
-0.008
-0.01
-0.012
0.03
0.04
0.05
0.06
m
500
450
400
350
300
250
200
150
100
50
(b)
350
300
250
200
150
100
50
z
y
x

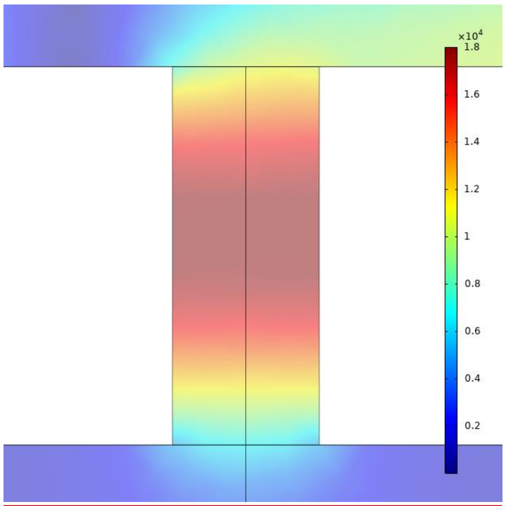

Figure 7 *: ~~(a)~~ Cross sectional view of the acoustic pressure field within a chamber excited by an ultrasonic sound source, with the inside of the chamber above and the open air below, both connected by the Fabry-Perot resonator. Pressure in ~~Pa. (b) Cross sectional view of the acoustic field within the resonator. Nozzle with suspended droplet included. Pressure in Pa~~Pa.*

The Fabry-Perot resonator simulation (Figure 7) shows a region of higher acoustic pressure forms within the resonator, as predicted. The acoustic pressure is highest in the center of the resonator, and tapers to a low value towards the two ends of the cylinder, resulting in a strong pressure gradient which can be used to exert an acoustophoretic force.~~The solution of the system displays a series of six pressure antinodes located in a periodic pattern on the surface of the chamber.~~

~~The Fabry-Perot resonator simulation (Figure 67) shows a region of higher acoustic pressure forms within the resonator, as predicted. The acoustic pressure is highest in the center of the resonator, and tapers to a low value towards the two ends of the~~

Formatted: Caption

Commented [JL98]: Should be 7 ?

Commented [LJ99R98]: Yes, that should be figure 7.

Formatted: Font: Not Bold

Commented [JL100]: Should be 7 ?

Commented [LJ101R100]: Yes, that should be figure 7.

~~cylinder, resulting in a strong pressure gradient which can be used to exert an acoustophoretic force.~~

This acoustophoretic force ~~is shown~~was found to be positive at~~for~~ the bottom half of the resonator by integrating the acoustic radiation force over the surface of the droplet, thanks to the previously mentioned pressure gradient. The pressure distribution in the cylinder (Figure 8) also matches that found in literature sources (~~Figure~~ Figure 3~~3~~), demonstrating the FEM simulation's capability to simulate subwavelength acoustic structures.

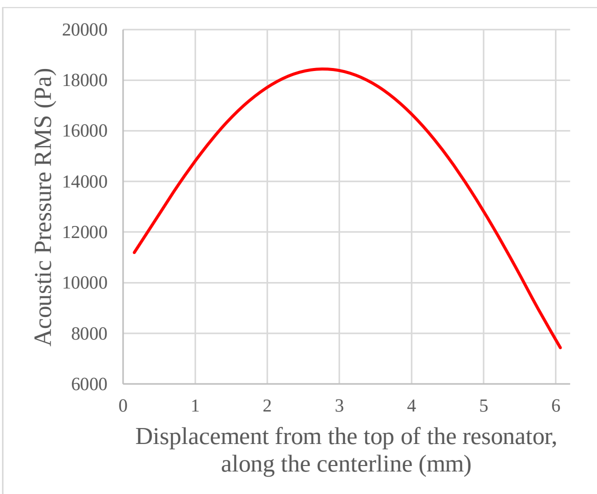

Figure 8 : Pressure distribution along centerline of the 6.2 mm long Fabry-Pérot resonator, moving from the top (inside of the chamber) to the bottom (outside of the chamber).

3.2.2. Resonator Array Simulation

The resonator array simulation required one hundred and twenty evaluations of the model to converge to a solution with the Nelder-Mead algorithm. With those

Formatted: Font: Not Italic

Formatted: Font: Not Bold, Check spelling and grammar

Field Code Changed

Commented [JL102]: Please plot the pressure distribution, in a figure included here

Commented [LJ103R102]: Added figure

Formatted: Font: Not Bold

Field Code Changed

Formatted: Centered, Keep with next

Formatted: Font: 14 pt, Bold, Font color: Auto

Formatted: Font: 14 pt, Font color: Auto

Formatted: Caption

Formatted: English (Canada)

parameters, all four resonators were maximally and equally excited by the single transducer.

The acoustic field within the chamber is illustrated in ~~Figure~~Figure 9~~ 8~~. We can see that the antinodes of pressure in ~~Figure~~ Figure 9~~8~~a correspond to antinodes of inverted magnitude in ~~Figure~~ Figure 9~~8~~c. Moreover, this figure shows clearly that the resonator ~~are~~is most excited ~~-~~when located in the areas of ~~low pressure~~low-pressure variation. ~~In those locations, while the sound pressure varies little, the air velocity is maximized; instead of antinodes of pressure, they are antinodes of air velocity. This gives us valuable information on how to excite the Fabry-Pérot resonators most effectively.~~

~~The plot shown in Figure 8b also clearly displays the periodic nature of this mode of vibration, with sixteen regularly spaced points of high pressure being clearly formed within the chamber on this plane.~~

Formatted: Font: Not Bold

Field Code Changed

Commented [JL104]: Do so for other sub-figures

Commented [LJ105R104]: Included mentions of each of the four subfigures.

Formatted: Font: Not Bold

Field Code Changed

Formatted: Font: Not Bold

Field Code Changed

Commented [JL106]: Rephrase.

Commented [LJ107R106]: Rephrased for clarity.

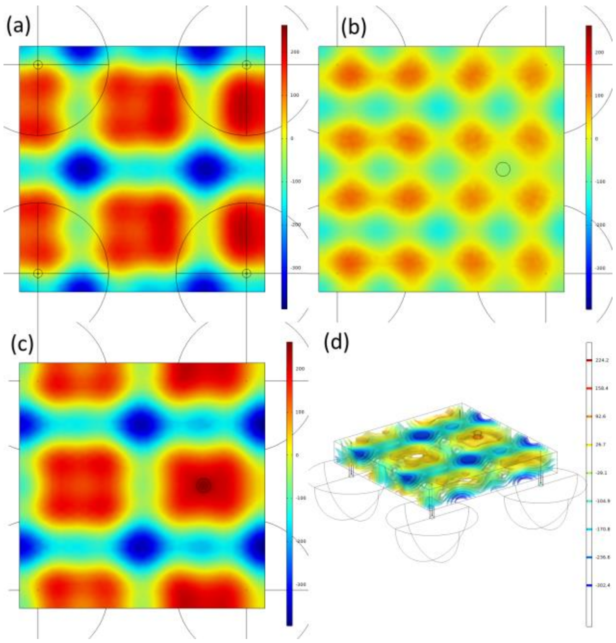

Figure *9~~8~~ : Plots representing the pressure field within the acoustic chamber designed to excite four resonators. All axes in units of Pascals. Plots (a), (b), and (c) show the acoustic pressure in the chamber on the bottom of the chamber (at the entrance of the resonators), halfway up the height of the acoustic chamber, and on the top surface of the acoustic chamber, respectively. Plot (d) shows the isosurface plot of the acoustic pressure within the chamber.* ~~*Pa?*~~

In those locations, the sound pressure varies little. In a standing wave, these points of constant pressure are instead where the air particle velocity varies the most. This gives us valuable information on how to excite the Fabry-Pérot resonators most effectively. We can draw from this that the opening of the resonator should be exposed to quickly moving particles to be excited optimally.

The plot shown in Figure 9b also displays the periodic nature of this mode of vibration, with sixteen regularly spaced points of high pressure being clearly formed

Formatted: Centered

Commented [JL108]: Rephrase.

Commented [LJ109R108]: Rephrased for clarity.

Formatted: Font: Not Bold

Formatted: Normal

within the chamber on this plane. This periodic pattern could potentially be extended to a larger chamber.

Formatted: English (Canada)

3.2.3. Resonant Chamber

The location and diameter of the transducer are denoted in ~~Figure~~ Figure 10~~9~~ by a transparent disc on the top surface of the chamber.

Formatted: Font: Not Bold

Field Code Changed

~~The FEM simulation of the air-filled chamber outputs a system with a set of pressure antinodes patterned at regular intervals alongside the edges and faces of the chamber, as seen in Figure 10a. Six antinodes are counted alongside a bottom edge of the chamber. The maximal pressure measured at a pressure antinode is 30.9 Pa. The centerline of the vessel also features a set of pressure antinodes.~~

Commented [JL110]: If figure 10 is mentioned first, it should be figure 9!!!!

Commented [JL111R110]: Avoid this issue in other places as well.

Commented [LJ112R110]: Figure 9 is now mentioned before figure 10.

Formatted: Centered

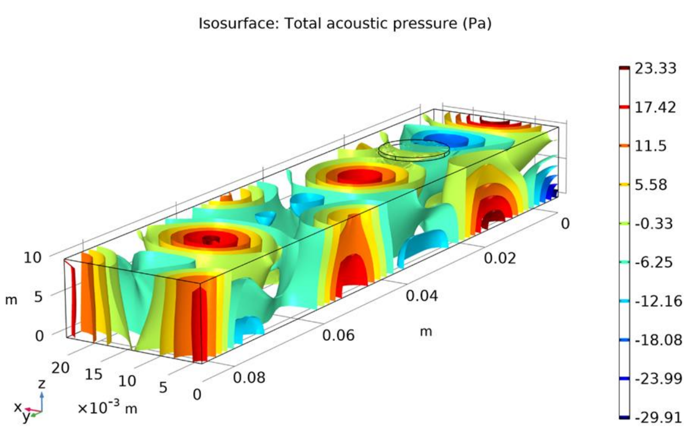

***Figure 10~~9~~** : Iso-surface plot of the total acoustic pressure within the air-filled chamber as solved by the finite element model.*

The FEM simulation of the air-filled chamber outputs a system with a set of pressure antinodes patterned at regular intervals alongside the edges and faces of the chamber, as seen in Figure 10. Six antinodes are counted alongside the bottom edge of the chamber. The maximal pressure measured at a pressure antinode is 30.9 Pa. The

Commented [JL113]: If figure 10 is mentioned first, it should be figure 9!!!!

Commented [JL114R113]: Avoid this issue in other places as well.

Commented [LJ115R113]: Figure 9 is now mentioned before figure 10.

Formatted: Font: Not Bold

centerline of the vessel also features a set of pressure antinodes.~~The location and diameter of the transducer are denoted in Figure 9 by a transparent disc on the top surface of the chamber.~~

The distance between the centers of the six antinodes and~~to~~ their neighbours are 17.2 mm. The wavelength of the soundwave is determined by $\lambda = c/f$, where c is ~~what,~~the speed of sound in the medium~~,~~ and f is ~~what…~~the frequency of the ultrasonic excitation. ~~meaning~~ T~~Tt~~he~~he~~ wavelength is calculated $\lambda = \frac{343m/s}{19850Hz} = 17.284\ mm$. This correspondence between the dimensions of the chamber and the wavelength is what leads to resonance within the volume.

Further insights into the geometry of the acoustic field can be found from ~~Studying~~ the isosurface plot (~~Figure~~ Figure 10~~9~~) of the pressure in the system~~ brings more insight into the geometry of the acoustic field~~. The two antinodes found in the center of a six-sided shape are actually the weaker side of pressure antinodes centered on the upper side of the chamber. Additionally, there are two types of antinodes in the system. There are stronger antinodes centered on specific points on the edges of the chamber, such as the eight antinodes found alongside the edges of the bottom surface of the chamber, and the four antinodes found alongside the centerline of the chamber on the upper surface of the chamber. ~~And there are w~~Weaker, more diffuse antinodes ~~which~~ are found in the volumes separating these antinodes. The pressure nodes, or the locations where the pressure variation is minimal, consist of the areas interstitial to the antinodes described above.

Formatted: Not Highlight

Formatted: Not Highlight

Formatted: Not Highlight

Formatted: Not Highlight

Formatted: Font: Not Bold

Field Code Changed

Commented [JL116]: Try to minimize the big white space due to the positioning of figures.

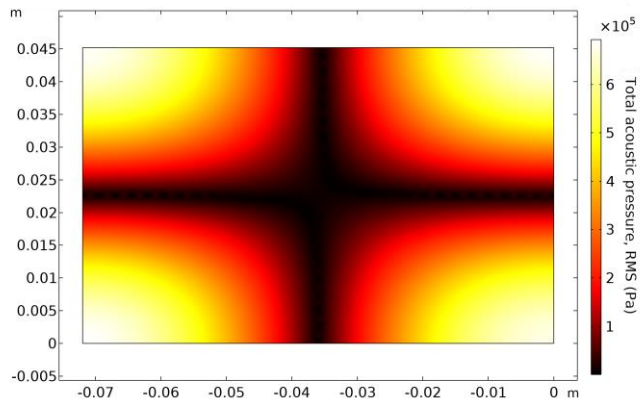

***Figure** 11~~10~~ : FEM simulation of water-filled chamber during excitation by transducer located in the upper right corner of the chamber. The RMS acoustic pressure in Pascals is plotted.*

~~And there are weaker, more diffuse antinodes which are found in the volumes separating these antinodes. The pressure nodes, or the locations where the pressure variation is minimal, consist of the areas interstitial to the antinodes described above.~~

~~*3.2.4. Water-filled Resonant Chamber*~~

~~In the water-filled chamber, the FEM simulation (Figure 10 and 11) resolves to a system of four antinodes located in the corners of the chamber. The maximal pressure is similar at each antinode. If cavitation is induced through the pressure variations in the chamber, this simulation predicts that cavitation will occur in all four corners. This strong resonance comes as a result of the main dimension of the vessel matching the wavelength of the soundwave (around 7.3 cm). This allows the formation of a standing wave system in the chamber.~~

Formatted: Centered

Commented [JL117]: And summarize and add the experimental reslt you have done. PRototypes the chamber and how, and the what is the problem. ALthough not successful, you can provide insights for future.

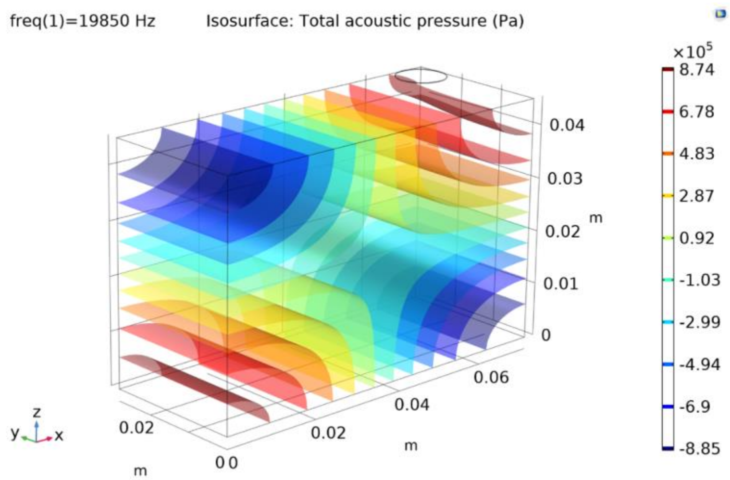

Figure ***12~~11~~*** *: FEM model of the water-filled chamber. Isosurface plot showing the sound pressure in Pascals.*

3.2.4. Water-filled Resonant Chamber

In the water-filled chamber, the FEM simulation (Figure 11 and 12) resolves to a system of four antinodes located in the corners of the chamber. The maximal pressure is similar at each antinode. If cavitation is induced through the pressure variations in the chamber, this simulation predicts that cavitation will occur in all four corners. This strong resonance comes as a result of the main dimension of the vessel matching the wavelength of the soundwave (around 7.3 cm). This allows the formation of a standing wave system in the chamber.

~~Unit?~~

Formatted: Centered

Commented [JL118]: Try to include into the maintexxt

Formatted: Normal, Line spacing: single

Chapter 4. Direct Measurement of Acoustic Fields and Cavitation Characterization through SCL

This chapter focuses on real-world experiments where high intensity ultrasonic soundwaves were applied to a variety of mediums. The first experiment, studying the acoustic field within an air-field resonant chamber, served to directly validate the results obtained in Chapter 3 by creating an analogous data set and measuring the error between the simulated acoustic field and the one observed empirically. The second ultrasound experiment will demonstrate the damping effect of large cavitation bubbles on the resonance of the chamber by comparing the cavitation observed through SCL in the chamber to the acoustic field computer in Chapter 3. Applications of the ultrasound in hydrogel polymerization are also investigated.~~[Introduce your research plan in this chapter. Provide a rationale that why you want to do the two experiments: acoustic field, cativation characterization? Why these two? How you argue combing them here. What are your questions to address in this chapter? What are the questions and objectives you want to address in this chapter? How is this chapter related to other chapters for cohesion of the]~~

Formatted: Not Highlight

Formatted: Not Highlight

Formatted: Normal

Formatted: Not Highlight

Formatted: Not Highlight

4.1. Experimental Section

4.1.1. Sound Pressure Measurement

A~~n~~ ~~ultrasonic transducer is was used as a~~ microphone suited for high frequency sound recording was used to record the sound pressure within the air-filled chamber, and its linear response output ~~is~~ was captured and processed using a data acquisition system (National Instruments, cDAQ-9172, cRIO-9233), and processed using LabVIEW (National Instruments, LabVIEW 2017). These raw pressure measurements ~~are~~ were then converted to root-mean-squared pressure to obtain a profile of the acoustic pressure within the chamber.

Commented [JL119]: What do you mean?

Commented [LJ120R119]: Reworded to be less confusing.

Commented [JL121]: Use past tense if you talked with the past experiments. Correct same issue in other places of the thesis

Commented [LJ122R121]: Changed to past tense when discussing experiments and methodology.

The acoustic chambers we~~a~~re constructed with 6.35 mm thick acrylic plate cut using a laser cutter (Universal Laser Systems, VLS3.75). The panels ~~are~~ were glued with a cyanoacrylate glue and waterproofed with silicon sealant for the water-filled chamber.

To measure the pressure inside the air-filled chamber without disrupting its resonance, a probe attachment for the microphone wa~~i~~s fabricated (~~Figure~~ Figure 13~~12~~). It consists of a nozzle (10 cm in length, 0.6 mm external diameter) (Polymicro, Fused Silica Capillary Tubing)~~ nozzle 10 cm in length~~, glued to an adapter manufactured to fit snugly on the tip of the microphone. This adapter blocks most pressure waves from reaching the microphone, allowing only pressure variations located at the tip of the nozzle to be measured. A thin~~ (~1 mm thick)~~ slit (~1 mm thick) wa~~i~~s cut into the narrow side of the air-filled chamber, allowing the probe to be swept across the entire bottom surface of the chamber while disrupting the acoustic field minimally.

Formatted: Font: Not Bold

Field Code Changed

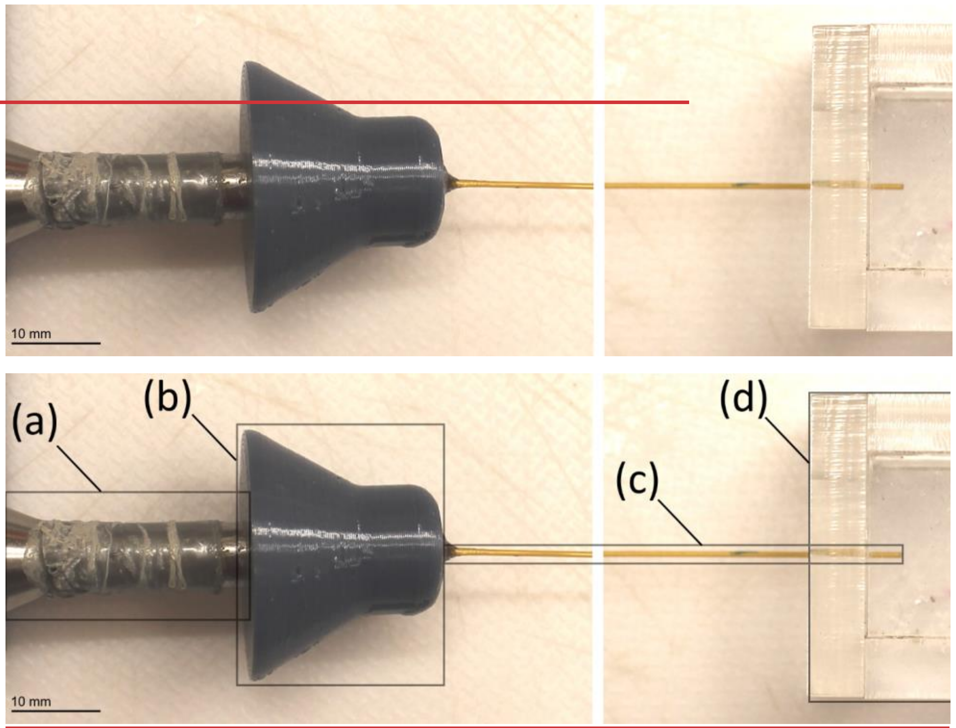

***Figure** 13~~12~~ : Probe microphone in chamber on the left, including 3D-printe~~r~~d adapter (b) attached to ultrasonic transducer (a) and fused silica tubing (c) glued to the adapter. On the right, the tip of the probe inserted through the side of the chamber (d).*

This microphone is swept along the whole length of the chamber at 16 equally-spaced lines along its width, resulting in a 2D mapping of the sound pressure of the surface. This motion is achieved by affixing the probe to a platform actuated in two direction by two stepper motors (Superior Electric, SLO-SYN Motor, M062-LS09), allowing for precise programmed movement. The entire surface of the vessel is swept in one recording at 50 kHz, moving the probe at ~~low speeds~~0.58 mm/s to ensure enough ~~points~~ data ~~are~~ is accumulated at each point in space to ensure an accurate RMS value can be calculated.

Commented [JL123]: Add a schematic, or clearly label in the figure each part

Commented [LJ124R123]: Added labels

Commented [JL125]: Info

Commented [LJ126R125]: Added motor info.

Commented [JL127]: What speed?

Commented [LJ128R127]: Added value for speed

4.1.2. Sonochemiluminescence

To characterize the presence of cavitation in the chamber, sonochemiluminescence (SCL) using a luminol solution was~~is~~ used. SCL provides a much stronger emission than simple sonoluminescence, allowing the detection of even small amounts of cavitation (*59*). Luminol ($C_8H_7N_3O_2$ 5-Amino-2,3-dihydrophthalazine-1,4-dione) can be used in a wide variety of imaging applications. For example, it is commonly used to measure detect glycated hemoglobin through purely chemical luminescence (*60*). Here, the luminescence of the luminol will be activated by the collapse of the cavitation bubble. ~~The solution is prepared by dissolving 1 mmol of luminol (Sigma Aldrich, 123072-5G), 0.1 mol of hydrogen peroxide (Sigma Aldrich, H1009-5ML) and 0.1 mol of EDTA (Sigma Aldrich, ED-100G) in 1 liter of 0.1 M sodium carbonate (Sigma Aldrich, 223530-500G). This solution is then adjusted to pH 12 through the addition of sodium hydroxide (Sigma Aldrich, 221465-1KG)~~ (*59*)~~. The SCL is observed using a DSLR camera (Nikon D5100) in a dark room. An exposure time of 5 minutes wasis used to balance the light detected from the SCL with the noise accumulated by the light sensor.~~

Commented [JL129]: Ref

Commented [LJ130R129]: Added reference.

Commented [JL131]: Provide more sentences discussing the use of SCL in literature here.

Commented [LJ132R131]: Added other uses.

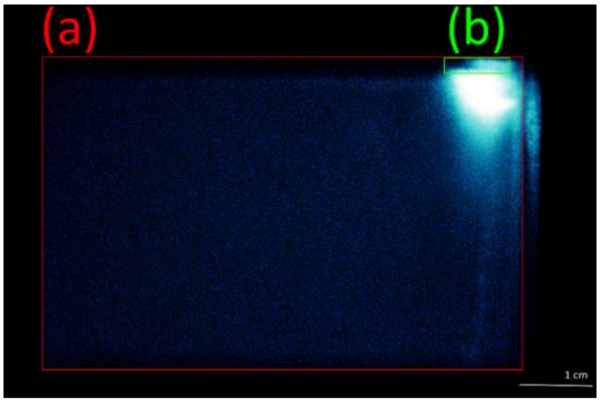

Figure* 14~~13~~ *: Real color imagery of the luminol solution-filled chamber recorded during sonication, 5 minutes exposure time. (a) is the bounds of the chamber, (b) is the location of the transducer horn.

The solution is prepared by dissolving 1 mmol of luminol (Sigma Aldrich, 123072-5G), 0.1 mol of hydrogen peroxide (Sigma Aldrich, H1009-5ML) and 0.1 mol of EDTA (Sigma Aldrich, ED-100G) in 1 liter of 0.1 M sodium carbonate (Sigma Aldrich, 223530-500G). This solution is then adjusted to pH 12 through the addition of sodium hydroxide (Sigma Aldrich, 221465-1KG) (*59*). The SCL is observed using a DSLR camera (Nikon D5100) in a dark room. An exposure time of 5 minutes was used to balance the light detected from the SCL with the noise accumulated by the light sensor.

4.1.3 Gel Polymerization Chambers

Two chambers were constructed for the gel polymerization experiments. The aim of the first chamber was to test the polymerization of multiple discrete hydrogels in a single experiment, without opening the vessel or requiring direct contact with the monomer solution. The second chamber is a test to investigate how far the polymerizing effect of the ultrasonic transducer can extend. Both used 0.25 inch thick lasercut acrylic plate sealed with silicone as its structural material. The first

Formatted: Keep with next

Commented [JL133]: You need to add some quantitative results here. For the image and video, you can plot the area/intensity as a function of time.

You can also include plot, showing the effect of US intensity

Commented [JL134R133]: Add chemical structure of the luminol

Commented [LJ135R133]: Added chemical structure above and more quantitative results and analysis in section 4.2.2.

Formatted: Normal

Commented [JL136]: Images?

You need to explain a bit about the design. For instance, closed chamber in order to avoid oxygen, which might inhibit polymerization.

Commented [JL137R136]: Schematic of this chamber

Commented [LJ138R136]: Added images and information on the design.

Formatted: Not Highlight

Formatted: Not Highlight

Formatted: Not Highlight

chamber (Figure 15~~Figure 15~~) had internal dimensions of 15 cm long by 3 cm wide by 1 cm tall, and its top surface was a thin PET film sheet, allowing acoustic waves to travel into the chamber without mixing the solutions inside and outside of the vessel. This vessel is filled with a polymerizable solution and sealed, and then immersed into a distilled water bath. The horn of the acoustic transducer is then pressed against the PET film at the location where ultrasonic excitation is desired.

The second chamber (Figure 16) is fully fabricated from laser acrylic plate with internal dimensions 6 cm by 5 cm by 1.5 cm. It has a single hole with diameter 0.375 inch through which the transducer horn can be inserted. It is designed to be filled with polymerizable solution and directly excited with the ultrasonic probe.

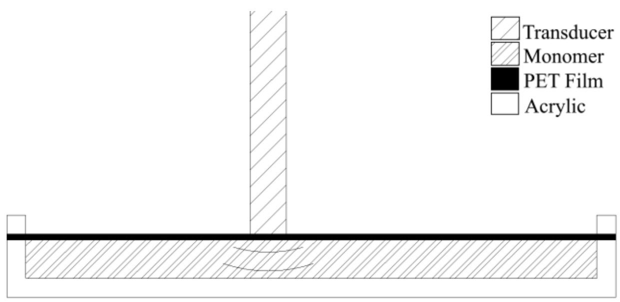

Figure 15 *: Chamber used in first gel polymerization experiment.*

Formatted: Font: Not Italic

Formatted: Font: Not Bold

Formatted: Font: Not Bold

Field Code Changed

Commented [JL139]: Given the figure content, you should adjust the size, ideally either half page, 3/4 page or whole page size

Commented [LJ140R139]: Adjusted figure dimensions to be appropriate for readability.

Formatted: Centered, Keep with next

Commented [JL141]: Make sure all figures are properly cited

Commented [LJ142R141]: These figures are original from this thesis.

Formatted: Font: 14 pt, Bold, Font color: Auto

Formatted: Font: 14 pt, Font color: Auto

Formatted: Font: 14 pt, Font color: Auto

Formatted: Caption

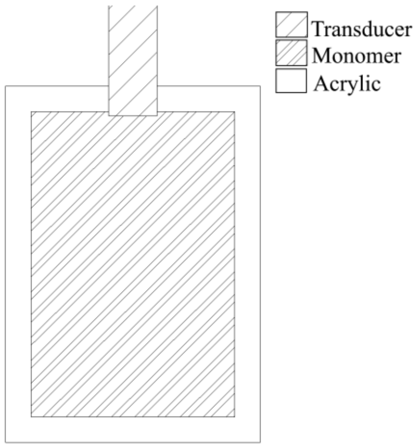

Formatted: Keep with next

Figure 16 : Chamber used in second gel polymerization experiment.

Formatted: Font: 14 pt, Bold, Font color: Auto

Formatted: Font: 14 pt, Bold, Font color: Auto

Formatted: Font: 14 pt, Font color: Auto

These chambers were designed to minimize contact between the atmosphere and the monomer solution, because atmospheric oxygen strongly inhibits the polymerization reaction by reacting with hydroxyl volatiles instead of the polymer reagents.

The reagents used in this monomer solution are acrylic acid-based monomer, PEGDA700 crosslinker, alginate, and glycerol, in an aqueous solution. This solution must be degassed to remove the oxygen dissolved within prior to the polymerization experiment.

4.2. Results and Discussion

4.2.1. Resonant Chamber Analysis and FEM Validation

The RMS sound pressure on the bottom face of the air-filled chamber is plotted in ~~Figure ~~Figure 17~~13~~b. The shape of the acoustic field has irregularities, but antinodes of pressure can be denoted. The long edges of the chamber each feature four higher amplitude antinodes, and two weaker, wider antinodes. The centerline features a pattern of varying pressure.

Formatted: Font: Not Bold

Field Code Changed

All the features denoted in the simulated acoustic pressure field (weak and strong antinodes, interstitial pressure nodes) can also be found in the empirical data, qualitatively demonstrating agreement between the measurements.

~~To quantify the correlation between the two results, we plot the relative error between the empirical and theoretical sound pressure with $Error\ Rate(\%) = \frac{P_{simulated} - P_{experimental}}{P_{experimental}}$ at every point of the surface (Figure 13c). An absolute relative error of under 50% is obtained on 52.7% of the surface, and observing the distribution of the smaller error regions, we can see they are localized around the antinodes of pressure.~~ ~~Observing this figure shows that the simulation tended to underestimate the pressure measured in lower pressure regions (pressure nodes) and overestimate it in some of the highest pressure regions (pressure antinodes). A portion of this difference may be attributable to small defects in the fabrication of the acoustic chamber, leading to a distortion of the acoustic field shape.~~

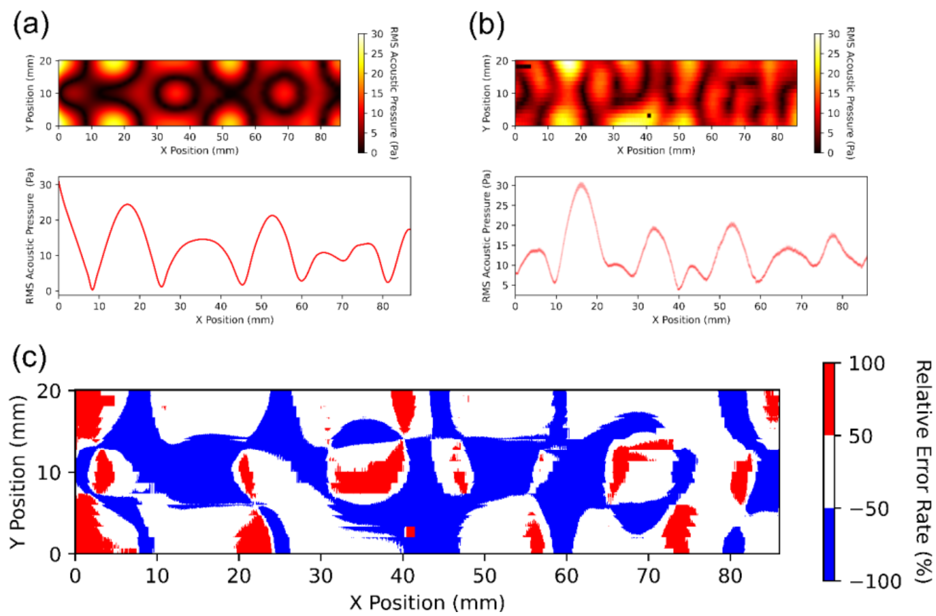

***Figure* 17~~13~~** *: Resonant chamber acoustic field comparative analysis. (a) Results of the FEM simulation of the air-filled acoustic chamber. The heatmap shows a regular pattern of pressure antinodes. The line plot below shows the pressure variation alongside a single edge of the vessel, displaying clearly peaks and troughs in the measurement. (b) RMS pressure measured with the probe microphone. The line plot below shows the pressure variation alongside a single edge of the vessel, displaying peaks and troughs in the measurement. (c) Mapping of the relative error between the empirical and experimental RMS pressure. Blue regions are where the simulated pressure was much lower than the experimental, red are where it was much higher, white are where it was within +/-50% of the value. Many topological features are captured in both, including the pressure antinodes and the two hexagon-shaped features at 36 and 70 mm alongside the X axis. ~~[spatial info of the antinode…]~~The spatial and geometry information of the pressure nodes and antinodes are of the most interest here.*

To quantify the correlation between the two results, we plot the relative error between the empirical and theoretical sound pressure with $Error\ Rate(\%) = \frac{P_{simulated} - P_{experimental}}{P_{experimental}}$ at every point of the surface (Figure 17c). An absolute relative

Formatted: Font: Not Bold

error of under 50% is obtained on 52.7% of the surface, and observing the distribution of the smaller error regions, we can see they are localized around the antinodes of pressure.

Observing this figure shows that the simulation tended to underestimate the pressure measured in lower pressure regions (pressure nodes) and overestimate it in some of the highest pressure regions (pressure antinodes). A portion of this difference may be attributable to small defects in the fabrication of the acoustic chamber, leading to a distortion of the acoustic field shape. For example, a planar misalignment of only a few degrees in one of the reflecting walls of the acoustic chamber can affect the geometry of the standing wave. This result shows that although the absolute pressure determined by the simulation differ from the empirical values, the geometry of the pressure field, including the location of nodes and antinodes of pressure, is replicated with good accuracy.

Other comparative studies of acoustic systems were found in the literature. Studies into the simulation of an ultrasonic sonoreactor (*61*) found a correlation between unidimensional empirical data and a corresponding numerical model (Figure 18), but our work finds good agreement in a system with a more complex acoustic field mapped in two dimensions. Other works study an acoustic field in multiple dimensions (Figure 1) and found agreement both quantitative and qualitative between their numerical and empirical data. The large number of data points gathered with our method allows our empirical data to capture more fine acoustic features that can be correlated with those found in the numerical model.

Commented [JL143]: What defects? Explain

Commented [LJ144R143]: Added explanation.

Formatted: Font: Not Bold

Field Code Changed

Formatted: Font: Not Bold

Field Code Changed

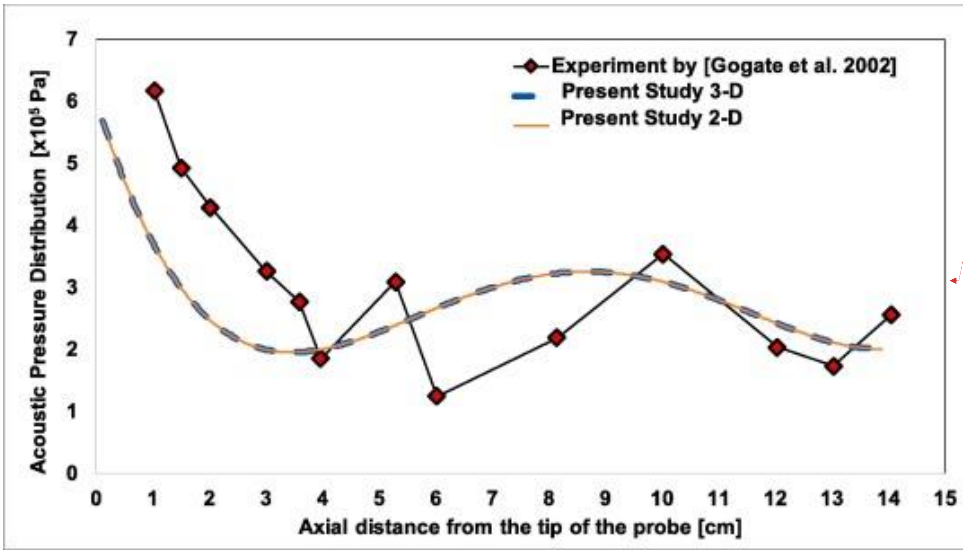

***Figure 18** : Validation of the numerical model of an ultrasonic sonoreactor with experimental results (Reproduced from (61), copyright 2020, Elsevier)*

~~[add a paragraph to discuss your results compared to the literature. Any similar studies in the literature, how good agreement and relative error did they report?]~~

4.2.2. SCL Imagery

SCL is observed in the luminol solution-filled vessel in ~~Figure~~ Figure 19~~14~~. It is localized below the transducer only. The area where cavitation is observed is projected in a diffuse cone below the tip of the transducer's horn.

Figure 19a and 19c show that the area where cavitation is observed tapers off more quickly in the horizontal direction (affected width of 1.32 cm) and more slowly in the vertical direction (affected height of 2.20 cm).

Formatted: Keep with next

Formatted: Font: 14 pt, Bold, Font color: Auto

Formatted: Font: (Default) Times New Roman, 14 pt, Font color: Auto

Formatted: Caption

Formatted: Highlight

Formatted: Font: Not Bold

Field Code Changed

Commented [JL145]: Again qualify the area. And present some quantitative results here.

The result interpretation of this experiment is insufficient clearly.

Commented [LJ146R145]: Added quantitative analysis of the result in figure 18

Formatted: Font: Not Bold

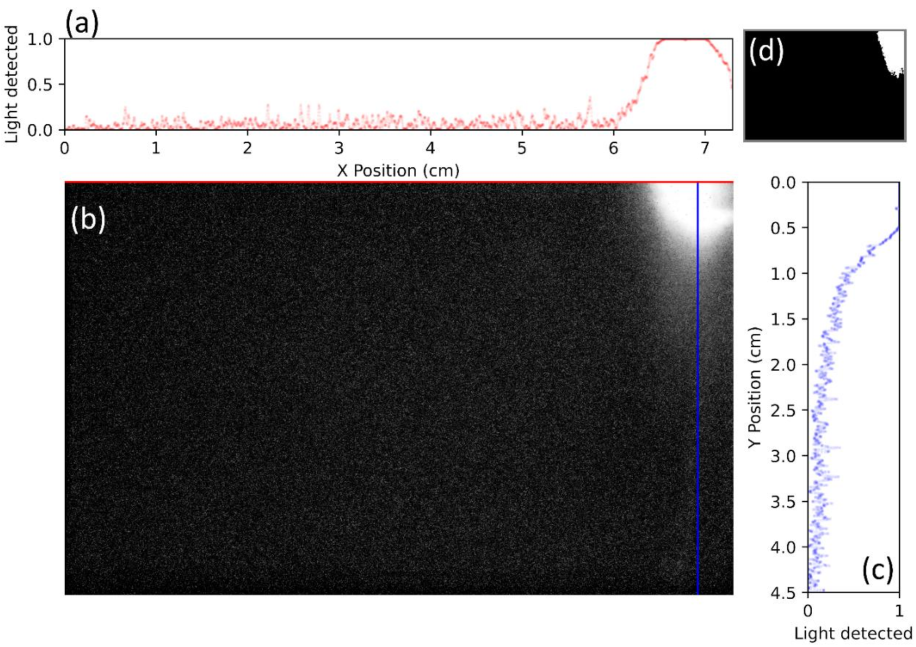

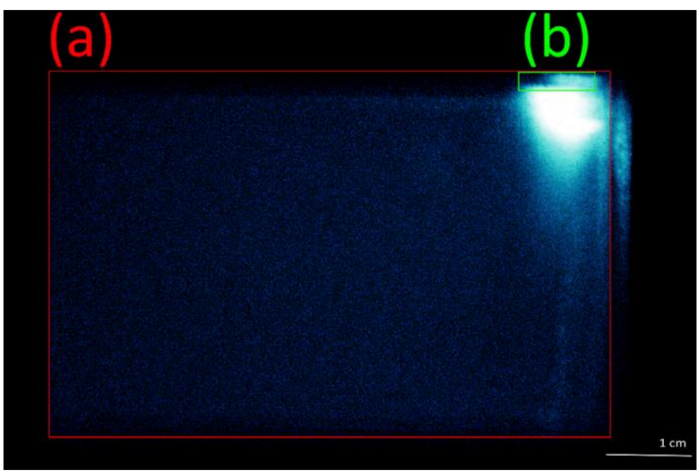

Figure 19~~181614~~ *: ~~Imagery of the luminol solution-filled chamber recorded during sonication, 5 minutes exposure time. (a) is the bounds of the chamber, (b) is the location of the transducer horn.~~Processed data output of SCL experiment. (b) shows*

Formatted: Centered

Formatted: Justified

Commented [JL147]: You need to add some quantitative results here. For the image and video, you can plot the area/intensity as a function of time.

You can also include plot, showing the effect of US intensity

Commented [JL148R147]: Add chemical structure of the luminol

Commented [LJ149R147]: Added quantitative analysis of are with cavitation and chemical structure of luminol in section 4.1.2.

the raw light information in monochrome. Data along the red line is plotted in (a) and data along the blue line is plotted in (c). (d) shows the area of the graph where the luminosity recorded is more than 20% higher than the base luminosity recorded in the dark parts of the image (attributed to sensor noise). This area represents 1.707 cm^2. The "Light detected" axes in (a) and (b) range from 0 to 1, above which the camera sensor was overexposed.

~~Figure 18Figure 16a and 1c show that the area where cavitation is observed tapers off more quickly in the horizontal direction (affected width of 1.32 cm) and more slowly in the vertical direction (affected height of 2.20 cm).~~ This can be attributed to the vertical motion of the transducer creating sound waves which are traveling through the medium vertically. On this 2D view of the chamber, the area where cavitation is measured is 1.707 cm^2 as seen in Figure 19d. If cavitation were distributed in all four corners of the chamber due to a standing wave system, the area where cavitation can be observed may be greater than this. This result demonstrates that cavitation bubbles have a disrupting effect on the formation of the acoustic wave in the resonant chamber, leading to a divergence to the result of the simulation, even while considering other nonlinear effects through the Westervelt equation. To be able to properly simulate this system, creating a simulation which explicitly accounts for the second (vapor) phase introduced by the bubbles may be necessary, as their effect on the traveling sound waves could then be properly expressed in the model.

4.3. Demonstration of Potential Applications

The results obtained in this chapter point to a variety of end applications for the systems investigated. Air-based acoustophoresis can be achieved through the use of the Fabry-Pérot resonators excited through acoustic chambers validated in 4.2.1. This type of acoustophoresis can be used to pull droplets from nozzles more flexibly than with other methods. This is accomplished by exploiting the gradient in acoustic pressure generated in the resonator. This gradient results in an unbalanced acoustic

Formatted: Font: 14 pt, Font color: Auto

Field Code Changed

Formatted: Font: Not Bold

radiation force which applies a net acceleration on the droplet, pushing it out of the resonator if its location is tuned properly.

Regarding the cavitation experiments, such cavitation phenomena could be used to induce hydrogel polymerization, which is a topic under study in ~~our group~~the Biomaterial Engineering research lab at McGill University. This experiment demonstrates successfully the effect of low-frequency bubbles on the resonance of a chamber, and methods to improve resonance remain to be investigated. Higher frequency ultrasonic soundwaves would more effectively induce polymerization of the gel, and our literature review (*44*, *45*, *61*) suggests these higher frequency soundwaves would be better able to form standing waves within the acoustic chamber, possibly leading to periodic patterns of polymerization as seen in ~~Figure 8~~Figure 9b. Creating such cellular hydrogels could lead to novel properties and new ways to engineer the mechanical properties of those materials.

Until high-frequency (~500 kHz as determined to be optimal for radical generation in (*45*)) experiments can be realized, polymerization experiments using the 20 kHz acoustic transducer have been completed. Two experiments were conducted. The second vessel described in section 4.1.3 was used to verify the polymerization of the solution when subjected to 5 minutes of high intensity ultrasonic excitation. A 5 centimeter long gel with tough hydrogel properties was synthesized in this manner and is shown in b. The first vessel was used to test the patterning of multiple discrete gels in a single vessel, which could be achieved by patterning areas of cavitation with a resonant acoustic field. Three gels are synthesized in a single experiment, and shown in a.

Commented [JL150]: Present some results here. It is ok to use some photos and images of sono-prepared gels you did with Yixun

Commented [LJ151R150]: Added figure for gels.

Formatted: Font: Not Bold

Field Code Changed

Field Code Changed

Field Code Changed

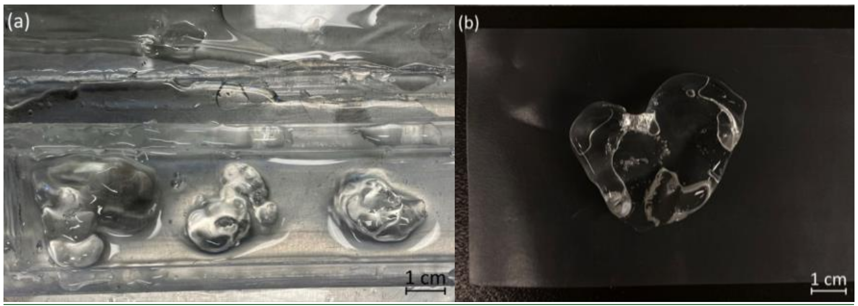

Figure 20 : Images of hydrogels polymerized using ultrasound. (a) Set of three hydrogels polymerized in a closed vessel by applying an ultrasonic excitation for 5 minutes to a solution through the PET film at three points separated from each other by three centimeters. (b) Gel polymerized in a vessel through direct application of an ultrasonic excitation for 5 minutes.

The hydrogel samples obtained are irregular in shape and have heterogeneous properties due to the gradient in volatiles generated by the transducer moving away from the horn. Applying the cavitation effects with a standing wave generated with a higher frequency ultrasonic sound source could help address both of those effects by distributing the radicals more evenly in the solution. The 20 kHz agitation also induces strong jet flows in the solution which contributed to breaking up the hydrogel. Higher frequency sound would impart less momentum to the fluid, reducing this effect and possibly improving the integrity of the hydrogel. New and improved hydrogel manufacturing methods could be developed by combining an engineered resonant acoustic field with a gel polymerized through sonochemistry, as the polymerization of the gel could be tuned by patterning antinodes of pressure where cavitation is most intense.

Commented [JL152]: Add a theme sentence to each figure caption

Commented [LJ153R152]: Added a sentence summarizing the figure to every figure with multiple subsections.

Formatted: Font: Italic

Formatted: Font: 14 pt

Formatted: Font: Italic

Formatted: Font: 14 pt, Italic

Formatted: Font: Italic

Formatted: Line spacing: single

Commented [JL154]: Add some information about the monomer, polymer. The chemical information.

Commented [JL155R154]: They can be included in the figure.

Commented [LJ156R154]: Added chemical information in 4.1.3.

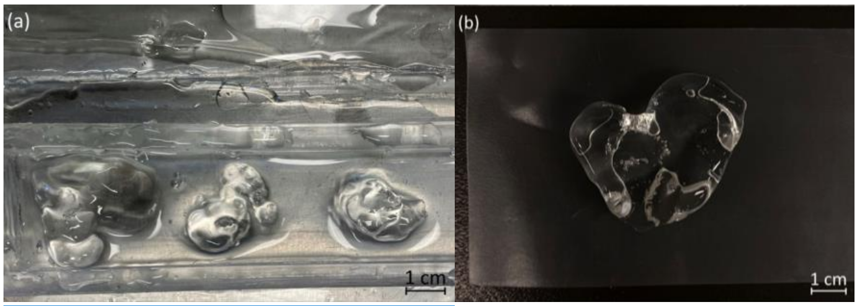

~~***Figure 1715*** *: Images of hydrogels polymerized using ultrasound. (a) Set of three gel polymerized in a closed vessel by applying an ultrasonic excitation for 5 minutes to a solution through the PET film at three point separated from each other by three centimeters. (b) Gel polymerized in a vessel through direct application of an ultrasonic excitation for 5 minutes.*~~

Formatted: Keep with next

Commented [JL157]: Add a theme sentence to each figure caption

Commented [LJ158R157]: Added a sentence summarizing the figure to every figure with multiple subsections.

Formatted: Caption

Chapter 5. Conclusion and Recommendations

5.1. Conclusion

In conclusion, ~~our work~~this thesis presents a ~~comprehensive~~ methodology for ~~simulating~~ modeling and utilizing tridimensional acoustic fields in resonant chambers, particularly focusing on high amplitude ultrasonic excitations. These excitations are of significant interest due to their wide range of applications in acoustophoretics, contactless ablation, and sonochemistry. We successfully incorporated the nonlinear effects of such interactions using the Westervelt equations, resulting in a remarkable agreement between the simulated acoustic field of an air-filled chamber and that of an identical empirical system. We also used SCL to show the Westervelt equation is not sufficient to simulate systems where cavitation bubbles are a major component of the bulk fluid. Moreover, a simulation of a subwavelength resonator and its agreement with results found in literature shows the technique is not limited to acoustic formations larger than the wavelength in dimension.

Overall, our research represents a step towards a better understanding of tridimensional acoustic fields in resonant chambers and paves the way for advancements in fields reliant on acoustic interactions. By refining this methodology and exploring additional nuances related to cavitation and frequency effects, we can further enhance the accuracy and applicability of those simulations in practical scenarios. These advancements have the potential to catalyze innovations in areas such as biomedical applications, material processing, and non-invasive medical procedures, thereby expanding the horizons of acoustics research and its transformative potential in the broader scientific community.

~~Developing a methodology to measure the sound pressure in the entire volume of a resonant acoustic chamber instead of only a surface could allow for a more thorough validation of the model, including the quantification of pressure antinodes which are not bound to one of the internal faces of the chamber. Regarding cavitation, there is evidence in the literature~~ (*62*) ~~that higher frequency sound sources may be better able to create a standing wave by generating smaller cavitation bubbles and fewer high-velocity microjets, both of which could improve traveling wave transmission through a medium undergoing cavitation.~~

5.2. Recommendations

Future work ~~in~~ of this project will include completing pressure mappings for acoustic chambers undergoing cavitation, and developing a multi-phase FEM model which better replicates the acoustic field in cavitating fluid. Developing a methodology to measure the sound pressure in the entire volume of a resonant acoustic chamber instead of only a surface could allow for a more thorough validation of the model, including the quantification of pressure antinodes which are not bound to one of the internal faces of the chamber. Multiple excitation frequencies would be tested to ascertain the effects of cavitation frequency on the standing wave, including higher frequency soundwave. Additionally, resonant chambers could be designed for explicit sono-synthesis~~chemical~~ purposes, such as ultrasound-mediated gel polymerization (*62*), which could allow for the periodic patterning of the gel's mechanical properties. ~~Developing a methodology to measure the sound pressure in the entire volume of a resonant acoustic chamber instead of only a surface could allow for a more thorough validation of the model, including the quantification of pressure antinodes which are not bound to one of the internal faces of the chamber.~~ Regarding cavitation, there is evidence in the literature (*63*) that higher frequency sound sources may be better able to create a standing wave by generating smaller cavitation bubbles and fewer high-velocity microjets, both of which could improve traveling wave transmission through a medium undergoing cavitation.

~~Overall, our research represents a step towards a better understanding of tridimensional acoustic fields in resonant chambers and paves the way for advancements in fields reliant on acoustic interactions. By refining this methodology and exploring additional nuances related to cavitation and frequency effects, we can further enhance the accuracy and applicability of those simulations in practical scenarios. These advancements have the potential to catalyze innovations in areas such as biomedical applications, material processing, and non-invasive medical procedures, thereby expanding the horizons of acoustics research and its transformative potential in the broader scientific community.~~

5.3. Original Contributions to Knowledge

This ~~present paper~~thesis makes a set of original knowledge contributions to the study of tridimensional ultrasonic acoustic fields. First, it presents a comparative analysis of the acoustic field inside a closed, air-filled resonant acoustic chamber. The experimental data gathered covers an entire 2D surface of the acoustic chamber in two dimensions, and is compared to an FEM-based simulation developed specifically for this acoustic chamber. Good agreement between the experimental mapping of the acoustic pressure field and the results of the simulation is found, both qualitatively in the topology of the standing wave, and quantitatively in the magnitude of pressure developed inside the chamber.

Second, t~~T~~he model studying an acoustic chamber outfitted with an array of resonators demonstrated that a two-dimensional periodic array of acoustic field features can be generated and optimized through the use of numerical methods. This control over the geometry of the acoustic field has the potential to lead to novel methods to engineer the properties of materials synthesized through the use of acoustic waves.

~~Second~~Third, the hypothesis that some cavitation fields can inhibit the formation of the standing wave is posited. To verify this, a matching acoustic chamber and simulation pair is constructed and designed. A strong standing wave field is observed in the simulation, but SCL imagery of the cavitation within the chamber shows the cavitation remained located beneath the sound source, demonstrating the disrupting effect of the cavitation on the standing wave. These findings point out the direction of future research.

References

1. S. P. Zhang *et al.*, Digital acoustofluidics enables contactless and programmable liquid handling. *Nature commun* **9**, 2928 (2018).
2. H. Bilal, M. Afzal, Reflection and transmission of acoustic waves through the bridging membrane junctions. *Wave Random Complex*, 1-24 (2022).
3. K. V. Vlassakov, X. Sala-Blanch, in *Nerves and Nerve Injuries,* R. S. Tubbs *et al.*, Eds. (Academic Press, San Diego, 2015), pp. 227-250.
4. T. Laurell, A. Lenshof, *Microscale acoustofluidics*. (Royal Society of Chemistry, 2014).
5. D. Foresti *et al.*, Acoustophoretic printing. *Sci Adv* **4**, eaat1659 (2018).
6. E. Undvall Anand *et al.*, Two-Step Acoustophoresis Separation of Live Tumor Cells from Whole Blood. *Analytical Chemistry* **93**, 17076-17085 (2021).
7. F. Petersson, L. Åberg, A.-M. Swärd-Nilsson, T. Laurell, Free flow acoustophoresis: microfluidic-based mode of particle and cell separation. *Anal. Chem.* **79**, 5117-5123 (2007).
8. R. Weser *et al.*, Three-dimensional heating and patterning dynamics of particles in microscale acoustic tweezers. *Lab Chip* **22**, 2886-2901 (2022).
9. S. Mohanty, I. S. M. Khalil, S. Misra, Contactless acoustic micro/nano manipulation: a paradigm for next generation applications in life sciences. *Proc R Soc A* **476**, 20200621 (2020).
10. J.-P. Franc, J.-M. Michel, *Fundamentals of cavitation*. (Springer science & Business media, 2006), vol. 76.
11. M. Ashokkumar, The characterization of acoustic cavitation bubbles – An overview. *Ultrason Sonochem* **18**, 864-872 (2011).
12. K.-H. Kim, G. Chahine, J.-P. Franc, A. Karimi, *Advanced experimental and numerical techniques for cavitation erosion prediction*. (Springer, 2014), vol. 106.
13. R. N. Weller, J. M. Brady, W. E. Bernier, Efficacy of ultrasonic cleaning. *Journal of endodontics* **6**, 740-743 (1980).
14. T. J. Mason, Ultrasonic cleaning: An historical perspective. *Ultrason Sonochem* **29**, 519-523 (2016).
15. A. Henglein, C. Kormann, Scavenging of OH radicals produced in the sonolysis of water. *Int J Radiat Biol* **48**, 251-258 (1985).
16. A. Weissler, Formation of hydrogen peroxide by ultrasonic waves: free radicals. *JACS* **81**, 1077-1081 (1959).
17. R. J. Siegel *et al.*, Ultrasonic plaque ablation. A new method for recanalization of partially or totally occluded arteries. *Circulation* **78**, 1443-1448 (1988).
18. C. K. Kim, B. K. Park, H. M. Lee, S. S. Kim, E. Kim, MRI techniques for prediction of local tumor progression after high-intensity focused ultrasonic ablation of prostate cancer. *American Journal of Roentgenology* **190**, 1180-1186 (2008).
19. R. Jeans, I. Mathews, The wave superposition method as a robust technique for computing acoustic fields. *J Acoust Soc Am* **92**, 1156-1166 (1992).

Formatted: Font: 16 pt

20. G. H. Koopmann, L. Song, J. B. Fahnline, A method for computing acoustic fields based on the principle of wave superposition. *J Acoust Soc Am* **86**, 2433-2438 (1989).

21. S. Zhao, J. Wallaschek, A standing wave acoustic levitation system for large planar objects. *Arch Appl Mech* **81**, 123-139 (2011).

22. J. J. Hawkes, W. T. Coakley, Force field particle filter, combining ultrasound standing waves and laminar flow. *Sens Actuators, B* **75**, 213-222 (2001).

23. D. Stanzial, D. Bonsi, G. Schiffrer, Four-dimensional treatment of linear acoustic fields and radiation pressure. *Acta Acust united Acust* **89**, 213-224 (2003).

24. C. Bailly, D. Juve, in *5th AIAA/CEAS aeroacoustics conference and exhibit*. (1999), pp. 1872.

25. J. A. Mann III, J. Tichy, A. J. Romano, Instantaneous and time‐averaged energy transfer in acoustic fields. *J Acoust Soc Am* **82**, 17-30 (1987).

26. H. Berktay, Possible exploitation of non-linear acoustics in underwater transmitting applications. *J Sound Vib* **2**, 435-461 (1965).

27. M. M. Karzova *et al.*, Shock formation and nonlinear saturation effects in the ultrasound field of a diagnostic curvilinear probe. *J Acoust Soc Am* **141**, 2327 (2017).

28. Z. Wei, L. K. Weavers, Combining COMSOL modeling with acoustic pressure maps to design sono-reactors. *Ultrason Sonochem* **31**, 490-498 (2016).

29. M. Solovchuk, T. W. Sheu, M. Thiriet, Simulation of nonlinear Westervelt equation for the investigation of acoustic streaming and nonlinear propagation effects. *J Acoust Soc Am* **134**, 3931-3942 (2013).

30. L. Bjørnø, Introduction to nonlinear acoustics. *Physics Procedia* **3**, 5-16 (2010).

31. L. V. King, On the acoustic radiation pressure on spheres. *Proc R Soc A* **147**, 212-240 (1934).

32. S. L. Garrett, in *Understanding Acoustics: An Experimentalist's View of Sound and Vibration,* S. L. Garrett, Ed. (Springer International Publishing, Cham, 2020), pp. 673-698.

33. J. Y. Wen, E. A. Habets, P. A. Naylor, in *2008 IEEE International Conference on Acoustics, Speech and Signal Processing*. (IEEE, 2008), pp. 329-332.

34. P. Ertl, D. Sticker, V. Charwat, C. Kasper, G. Lepperdinger, Lab-on-a-chip technologies for stem cell analysis. *Trends Biotechnol* **32**, 245-253 (2014).

35. G. Balázs *et al.*, Advantages and limitation of lab-on-a-chip technique in the analysis of wheat proteins. *Cereal Res Commun* **40**, 562-572 (2012).

36. L. Meng *et al.*, Acoustic tweezers. *J Phys D: Appl Phys* **52**, 273001 (2019).

37. X. Ding *et al.*, Surface acoustic wave microfluidics. *Lab Chip* **13**, 3626-3649 (2013).

38. R. Sauleau, Fabry–perot resonators. *Encyclopedia of RF and microwave engineering*, (2005).

39. J. Christensen, L. Martin-Moreno, F. J. Garcia-Vidal, Theory of resonant acoustic transmission through subwavelength apertures. *Phys Rev Lett* **101**, 014301 (2008).

40. J. U. Park *et al.*, High-resolution electrohydrodynamic jet printing. *Nat Mater* **6**, 782-789 (2007).

41. B. Derby, Inkjet printing of functional and structural materials: fluid property requirements, feature stability, and resolution. *Annu Rev Mater Res* **40**, 395-414 (2010).

42. N. S. M. Yusof, S. Anandan, P. Sivashanmugam, E. M. M. Flores, M. Ashokkumar, A correlation between cavitation bubble temperature, sonoluminescence and interfacial chemistry - A minireview. *Ultrason Sonochem* **85**, 105988 (2022).

43. P. Riesz, D. Berdahl, C. L. Christman, Free radical generation by ultrasound in aqueous and nonaqueous solutions. *Environ Health Perspect* **64**, 233-252 (1985).

44. A. Brotchie, F. Grieser, M. Ashokkumar, Effect of Power and Frequency on Bubble-Size Distributions in Acoustic Cavitation. *Phys Rev Lett* **102**, 084302 (2009).

45. T. G. McKenzie, F. Karimi, M. Ashokkumar, G. G. Qiao, Ultrasound and Sonochemistry for Radical Polymerization: Sound Synthesis. *Chem Eur J* **25**, 5372-5388 (2019).

46. B. Würsig, C. R. Greene, Jr., T. A. Jefferson, Development of an air bubble curtain to reduce underwater noise of percussive piling. *Mar Environ Res* **49**, 79-93 (2000).

47. K. N. Long, T. F. Scott, H. Jerry Qi, C. N. Bowman, M. L. Dunn, Photomechanics of light-activated polymers. *J. Mech. Phys. Solids* **57**, 1103-1121 (2009).

48. J. Maitra, V. K. Shukla, Cross-linking in hydrogels-a review. *Am J Polym Sci* **4**, 25-31 (2014).

49. B. Kaltenbacher, I. Lasiecka, R. Marchand, Wellposedness and exponential decay rates for the Moore-Gibson-Thompson equation arising in high intensity ultrasound. *Control and Cybernetics* **40**, 971-988 (2011).

50. D. N. Arnold, F. Brezzi, B. Cockburn, D. Marini, in *Discontinuous Galerkin Methods,* B. Cockburn, G. E. Karniadakis, C.-W. Shu, Eds. (Springer Berlin Heidelberg, Berlin, Heidelberg, 2000), pp. 89-101.

51. B. Cockburn, Discontinuous Galerkin methods. *ZAMM* **83**, 731-754 (2003).

52. B. Olson, I. Hashmi, K. Molloy, A. Shehu, Basin Hopping as a General and Versatile Optimization Framework for the Characterization of Biological Macromolecules. *Adv. Artif. Intell.* **2012**, 674832 (2012).

53. M. A. Luersen, R. Le Riche, Globalized Nelder–Mead method for engineering optimization. *Comput. Struct.* **82**, 2251-2260 (2004).

54. J. Nelder, Nelder-Mead Method. *Comput. J.* **7**, 308-313 (1965).

55. W. Press, S. Teukolsky, W. Vetterling, B. Flannery. (Cambridge University Press New York, 2007).

56. H. Ghiasi, D. Pasini, L. Lessard, Constrained Globalized Nelder—Mead Method for Simultaneous Structural and Manufacturing Optimization of a Composite Bracket. *J. Compos. Mater.* **42**, 717-736 (2008).

57. A. S. Koigerov, A. V. Korlyakov, Finite Element Modeling of Surface Acoustic Wave Devices Using COMSOL. *Russian Microelectronics* **51**, 226-235 (2022).

58. J. Lei, M. Hill, P. Glynne-Jones, Numerical simulation of 3D boundary-driven acoustic streaming in microfluidic devices. *Lab Chip* **14**, 532-541 (2014).

59. G. J. Price, N. K. Harris, A. J. Stewart, Direct observation of cavitation fields at 23 and 515 kHz. *Ultrason Sonochem* **17**, 30-33 (2010).

60. K.-S. Ahn, J. H. Lee, J.-M. Park, H. N. Choi, W.-Y. Lee, Luminol chemiluminescence biosensor for glycated hemoglobin (HbA1c) in human blood samples. *Biosens. Bioelectron.* **75**, 82-87 (2016).

61. S. S. Rashwan, I. Dincer, A. Mohany, Investigation of acoustic and geometric effects on the sonoreactor performance. *Ultrason Sonochem* **68**, 105174 (2020).

62. Z. Ma *et al.*, Controlled tough bioadhesion mediated by ultrasound. *Science* **377**, 751-755 (2022).

63. D. Sunartio, M. Ashokkumar, F. Grieser, Study of the Coalescence of Acoustic Bubbles as a Function of Frequency, Power, and Water-Soluble Additives. *JACS* **129**, 6031-6036 (2007).